Lack of continuity of the San Andreas Fault in southern California: Three-dimensional fault models and earthquake scenarios

Sara Carena and John Suppe
Department of Geosciences, Princeton University, Princeton, New Jersey, USA

Honn Kao
Pacific Geoscience Centre, Geological Survey of Canada, Sidney, British Columbia, Canada

Received 20 June 2003; revised 15 January 2004; accepted 6 February 2004; published 28 April 2004.

[1] The 1200-km-long San Andreas Fault loses its apparent continuity in southern California near San Gorgonio Pass [*Allen*, 1957], which raises significant questions given the dominant role of this fault in active California tectonics. What is the fundamental three-dimensional (3-D) geometry and kinematic behavior of the San Andreas fault system in this complex region? Is a throughgoing, if complex, San Andreas rupture from the Mojave Desert to the Coachella Valley possible? We have explored the issue of 3-D continuity by mapping over 60 faults in this region to depths of 15–20 km from hypocenter locations and focal mechanisms. We were able to constrain the 3-D geometry of the San Andreas fault zone (SAF) near San Gorgonio Pass from the 3-D geometry of the fault network surrounding it. The most likely configuration is for the San Andreas Fault to merge into the shallow-dipping San Gorgonio Pass thrust northwest of Indio. We concluded that there is no direct continuity at present but rather a network of faults, and the only kind of rupture possible for the SAF in this region is a complex rupture, involving both strike-slip and reverse faulting. GPS measurements also suggest that despite the fact that large motions must have occurred in the past based on offset geologic markers, only minor motion is occurring today in this area. Applying our findings about the fault geometry, we explored several simple earthquake scenarios to determine the most favorable conditions for a throughgoing rupture of the San Andreas fault system from the Mojave Desert to the Coachella Valley. *INDEX TERMS:* 7205 Seismology: Continental crust (1242); 7223 Seismology: Seismic hazard assessment and prediction; 7230 Seismology: Seismicity and seismotectonics; 8107 Tectonophysics: Continental neotectonics; 8010 Structural Geology: Fractures and faults; *KEYWORDS:* San Gorgonio Pass, San Andreas Fault, southern California

Citation: Carena, S., J. Suppe, and H. Kao (2004), Lack of continuity of the San Andreas Fault in southern California: Three-dimensional fault models and earthquake scenarios, *J. Geophys. Res.*, *109*, B04313, doi:10.1029/2003JB002643.

1. Introduction

[2] The continuity of the active, 1200-km-long San Andreas fault system is interrupted at the surface in very few places, the most notable of which is the 80-km-long step over between Cajon Pass to the northwest and San Gorgonio Pass to the southeast [*Allen*, 1957] (Figure 1). In recent years, there have been several attempts to answer two long-standing fundamental questions regarding this stretch of the San Andreas Fault. Is the San Andreas Fault continuous and vertical throughout? Is a San Andreas rupture from the Mojave Desert to Coachella Valley possible? The answers to these questions have fundamental implications for earthquake hazards in the Los Angeles region. Several authors have given important contributions toward answering the first question by producing models of the fault geometry from a variety of data and observations, resulting in a mix of "yes" and "no" answers [e.g., *Morton and Matti*, 1993; *Seeber and Armbruster*, 1995; *Magistrale and Sanders*, 1996; *Spotila and Sieh*, 2000; *Yule and Sieh*, 2001, 2003].

[3] Here we present new constraints on this problem using methods developed by *Carena and Suppe* [2002] and *Carena et al.* [2002], making use of the vast number of routinely recorded small earthquakes that constitute the bulk of the regional catalog, combined with surface traces and land morphology and some subsurface geologic data, to construct digital three-dimensional (3-D) surfaces of active faults. We apply these methods to first obtain a detailed geometry of the San Andreas fault system in the vicinity of San Gorgonio Pass, and then use the results to explore the possibility of the San Andreas Fault rupturing all the way through from the Mojave Desert to Coachella Valley.

[4] All the earthquake data and the 3D fault models we produced will be available in the database of the SCEC

0148-0227/04/2003JB002643$09.00

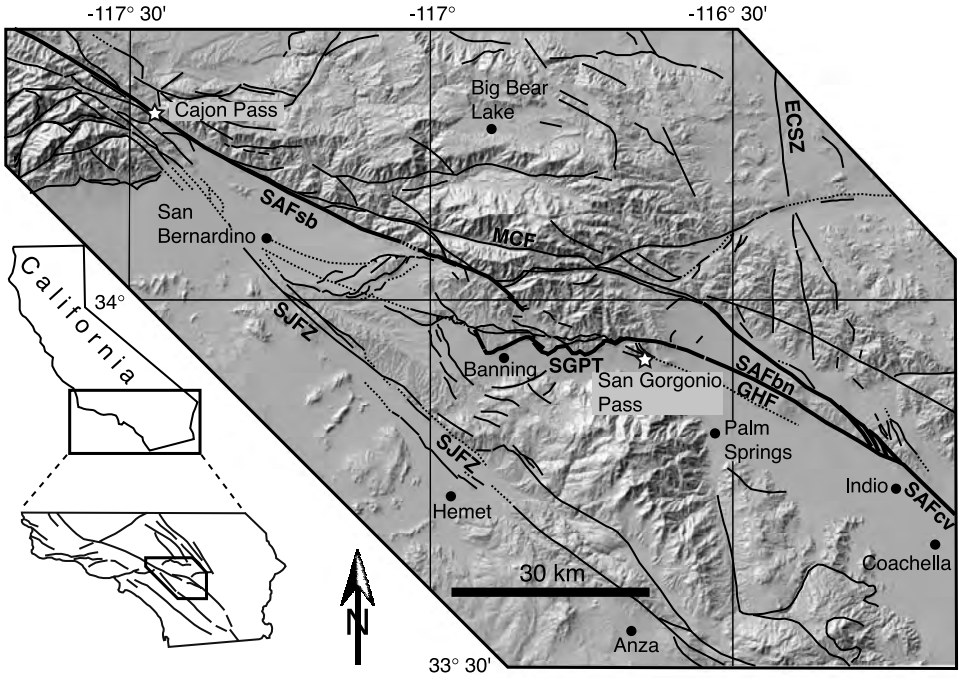

Figure 1. Location maps. Fault traces are from *Morton and Matti* [1993], *Jennings* [1994], and *Yule and Sieh* [2003]. SAFsb, San Bernardino segment of the San Andreas Fault; MCF, Mill Creek fault; SGPT, San Gorgonio Pass thrust; SAFcv, Coachella Valley segment of the San Andreas Fault; SJFZ, San Jacinto fault zone; ECSZ, eastern California shear zone; SAFbn, Banning segment of the San Andreas Fault; GHF, Garnet Hill fault.

Community Fault Model (CFM, http://structure.harvard.edu/cfma).

2. Tectonic Setting and Previous Models

[5] The plate boundary between the North American and the Pacific plates is particularly complex in southern California. Two major converging fault zones, the San Andreas fault zone (SAF) and the San Jacinto fault zone (SJFZ), dominate the area south of Cajon Pass (Figure 1). To the northeast, the eastern California shear zone (ECSZ) is another prominent tectonic feature. While the San Andreas Fault is generally identified with the plate boundary, the plate motion accommodated by the SJFZ and by the ECSZ is not negligible [*Morton and Matti*, 1993; *Shen et al.*, 1997; *Meade et al.*, 2002]. Recent studies show that at least 255 km of dextral slip must have occurred in southern California since 6.3 Ma to accommodate an equivalent amount of slip during the opening of the Gulf of California [*Oskin et al.*, 2001]. However, only about 150 to 190 km have occurred on the San Andreas Fault itself [*Matti et al.*, 1992; *Dickinson*, 1996]. The remainder is accounted for by slip on faults west of the San Andreas and slip on the ECSZ faults [*Dickinson*, 1996].

[6] Whereas most of the San Andreas fault zone north of Cajon Pass and south of Indio is more or less a continuous fault, the left step of the San Andreas near San Gorgonio Pass interrupts this continuity and gives rise to a complex fault network where it is not obvious which fault dominates [e.g., *Allen*, 1957; *Matti et al.*, 1985; *Morton and Matti*, 1993]. Southeast of Cajon Pass, the SAF splits into two main segments, the Mill Creek fault to the north (late Quaternary age, inactive probably since the late Pleistocene [*Matti et al.*, 1992]), and the San Bernardino segment to the south (formed in the late Pleistocene and currently active [*Matti et al.*, 1992; *Yule and Sieh*, 2001]).

[7] The region extending southeast from Cajon Pass to Indio has a very high level of seismicity on many faults but not on the San Andreas itself [*Petersen and Wesnousky*, 1994] (Figure 2a) (supplemented[1]). In fact, there is no clear evidence of the presence of the San Andreas at shallow levels east of Banning [*Allen*, 1957; *Matti et al.*, 1992]. *Magistrale and Sanders* [1996] consider it unlikely for the San Andreas to be continuous here even at depth, because the fault does not offset a marked step in seismicity (see earthquake depth changes in Figures 2a–2c) that they interpret as a lithological boundary.

[8] Two recent models for the geometry and kinematics of the SAF system near San Gorgonio Pass both include a complex combination of right-lateral strike-slip and thrust faulting: (1) *Seeber and Armbruster* [1995] consider the San Gorgonio Pass thrust an active fault that produces minor offsets at shallow depth in a mainly continuous vertical San Andreas Fault, based on their analysis of alignment of nodal planes and slip vectors in 3-D. (2) In contrast, *Yule and Sieh* [2003], on the basis of paleoseismological and geomorphologic observations, interpret the San Gorgonio Pass thrust as a shallow-dipping section of the San Andreas fault system,

[1] Auxiliary material is available at ftp://ftp.agu.org/apend/jb/2003JB002643.

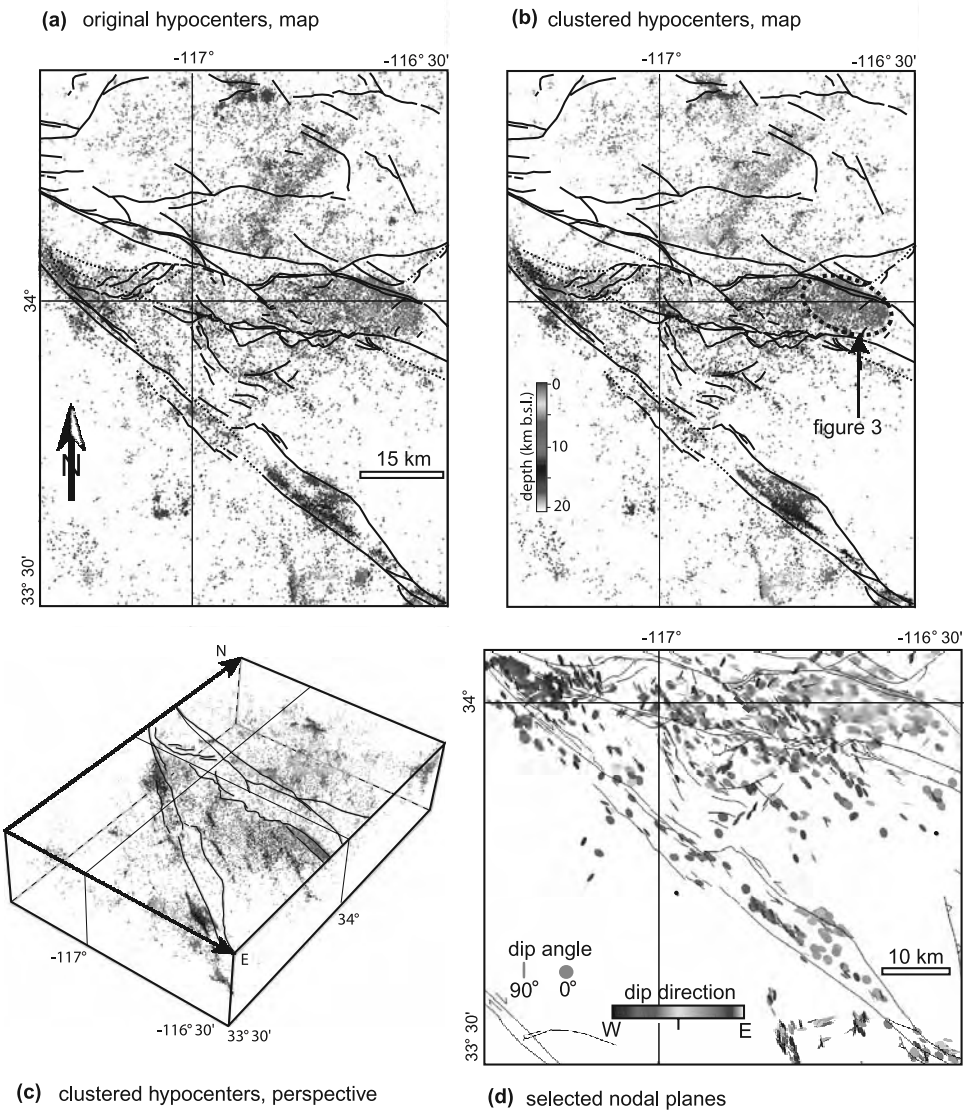

Figure 2. Data used in this paper. (a) Map of 43,000 events relocated by *Richards-Dinger and Shearer* [2000], before clustering. (b) Map of the same hypocenters after clustering. (c) The relocated hypocenters viewed in 3-D from the southeast. (d) Our selection of 1540 nodal planes from the focal mechanisms of *Hauksson* [2000]. This figure is supplemented by the "earthquake data" video. See color version of this figure at back of this issue.

excluding the presence of a vertical throughgoing San Andreas Fault.

[9] Unlike previous authors, we were able not only to visualize earthquake hypocenters and focal mechanisms in 3-D, but also fit structurally realistic fault surfaces to them and constrain these surfaces using additional information like focal mechanisms and mapped fault traces. Below we describe our methods and results, and then we experiment with different earthquake scenarios applied to our general solution for the 3-D geometry of the San Andreas fault system in this region.

3. Modeling Faults in 3-D

3.1. Data and Methods

[10] We use earthquake hypocenter locations to constrain our 3-D models of fault surfaces. For this work, we obtained the hypocenter location data of *Richards-Dinger and Shearer* [2000] from the Southern California Earthquake Center (SCEC) database (Figure 2a). This catalog contains 43,500 relocated events in our study area recorded in the period 1975–1998.

3.1.1. Processing and Constraints

[11] The hypocenter locations were then clustered using the "collapsing method" developed and described by *Jones and Stewart* [1997] and modified by *Nicholson et al.* [2000]. Clustering results in tighter hypocenter distributions (a "sharper" image, see Figures 2b–2c), which makes the process of selecting subsets of earthquakes much easier, and can illuminate details of the fault surface geometry otherwise masked by location errors. This method can be applied whenever information about location uncertainty is preserved in the catalog or is recoverable in some way, and when there is some overlap among earthquake uncertainty

ellipsoids. Both conditions are satisfied by the hypocenter locations of *Richards-Dinger and Shearer* [2000]. Before using the hypocenters for fault modeling, we removed those events that were likely to be quarry blasts.

[12] Fault geometry can be constrained by focal mechanisms as well. As demonstrated by *Seeber and Armbruster* [1995], focal mechanisms can be used to identify complex fault interactions even in areas of sparse seismicity. For this study, we used 13,000 focal mechanisms made available by *Hauksson* [2000] on the SCEC database. The comparison between earthquake hypocenter distribution and focal mechanisms in 3-D allowed us to (1) distinguish between principal and auxiliary nodal planes, thus making it possible to select only the principal planes and vectors in the data set (Figure 2d), (2) identify and map faults which have only a few events associated with them, (3) determine the current slip direction on several faults.

[13] A third type of constraint that can be applied to fault geometry is surface traces, either in the form of known breaks caused by a specific earthquake [*Carena and Suppe*, 2002], or as mapped fault traces. We combined the fault maps of *Matti et al.* [1992] and *Yule and Sieh* [2003] with the USGS digital elevation models to determine the 3-D shape of surface traces in the area of interest. Surface traces constrain the position of the top of the fault and may disclose a change in fault dip that could have gone undetected, since there are generally no or very few earthquakes at shallow depths.

3.1.2. Building 3-D Fault Surfaces

[14] In order to generate fault surfaces, we must be able to view and manipulate our data easily in 3-D. For this purpose, we chose to use gOcad, a 3-D Earth modeling software package. In addition to 3-D viewing capability, gOcad provides all the tools and functionalities needed to select clusters of earthquakes, fit reasonable fault surfaces to them, obtain fitting statistics, and include constraints in the fault models [*Mallet*, 2002; *Carena and Suppe*, 2002] (information on the gOcad project is located at http://gocad.ensg.inpl-nancy.fr). We start by identifying and separating clusters of earthquake hypocenters (Figure 3) that illuminate different faults. This is the most subjective part of the procedure, but in most cases the clusters are fairly obvious features when viewed in 3-D. Different people performing the selection could include or exclude a few different earthquakes, but in the majority of cases where there is a recognizable cluster, these differences are limited to the outer edges of the cluster. Because the steps that follow the selection always include some form of averaging of the hypocenter locations, small differences in the initial selection of hypocenters will not have any appreciable influence on the final fault geometry. If the fault being modeled has associated surface traces, they can be transformed into discrete points and included in the data set. These points on the surface trace are well located relative to the earthquakes and thus will be fixed spatial constraints (control nodes), meaning that in all subsequent manipulations of the fault surface these nodes will never be allowed to move.

[15] We then build fault surfaces from the identified clusters and the integrated additional data. A least squares inversion, where a plane is fitted to the cloud of points, is the simplest way to generate a fault surface. However, this would not be a structurally realistic fault surface. Most faults show changes in dip and/or strike, sometimes very marked, resulting in steps, bends, and other types of asperities, which have important implications for earthquake nucleation [*Shaw et al.*, 1994; *Carena and Suppe*, 2002] and deformation of the hanging wall block [e.g., *Suppe*, 1983; *Shaw and Shearer*, 1999]. For this reason we prefer to use irregular triangulated surfaces as the basis of fitting the hypocentral locations (Figure 3). More specifically, gOcad builds surfaces from sets of points using a Delaunay triangulation [*Delaunay*, 1934].

[16] Last, the surface is smoothed with the gOcad DSI algorithm [*Mallet*, 1992, 2002] (Figure 3). The smoothing will preserve any major feature of the surface, like changes in strike and dip, bends, steps, etc., but will smooth out all those minor ''bumps'' created by the fitting procedure that in most cases are the result of earthquake scattering due to original location errors not filtered out by the clustering algorithm. The result is a smooth surface that preserves the overall geometry of the hypocenter cluster, but eliminates the minor irregularities due to hypocenter scattering.

3.1.3. Model Resolution and Uncertainties

[17] The resolution of our fault models does of course depend on the original accuracy in the hypocenter locations [*Carena and Suppe*, 2002]. We do not attempt to resolve any structures or details of the fault surface smaller than the average hypocenter location uncertainties (which in this case is about 0.6 km in the horizontal plane and 1.8 km vertically), as any structures below this size could simply be artifacts. This has also implications for the definition of fault ''plane'' versus fault ''zone'': the distinction between the two is contingent upon the level of detail. As a matter of convenience, we call our models ''fault surfaces'', as most of them are defined by a band of earthquakes whose width is close to our resolution limit, and we cannot resolve any finer structures (such as closely spaced, parallel faults) within these bands. Our ''fault surface'' represents the middle of the illuminated fault zone, which typically corresponds to the maximum earthquake density.

[18] The example shown in Figure 3 (the aftershocks of the 1986 North Palm Springs earthquake) represents a good quality fault surface. It fulfills several criteria: there is a tight, dense hypocenter cluster with a width close to the resolution limit, a surface trace of the fault is available to constrain the top, and the 3-D geometry of the fault closely matches most of the available focal mechanisms. In this case over 95% of the clustered events (Figure 3a) fall within 2σ ($\pm$421 m) of the final fault model (Figures 3c and 3e). This distance is well below the average location uncertainties in the catalog of *Richards-Dinger and Shearer* [2000].

3.2. Fault Geometry

[19] We modeled 60 faults and fault segments from the clustered hypocenters alone (Figures 4–7). Some fault surfaces were extended beyond the area illuminated by earthquakes using information about surface traces and focal mechanisms. For example, the ''footwall faults'' in Figure 6 are shown extending to the surface in Figure 7. Even though these structures are not currently illuminated by earthquakes at depths shallower than 6–7 km, their

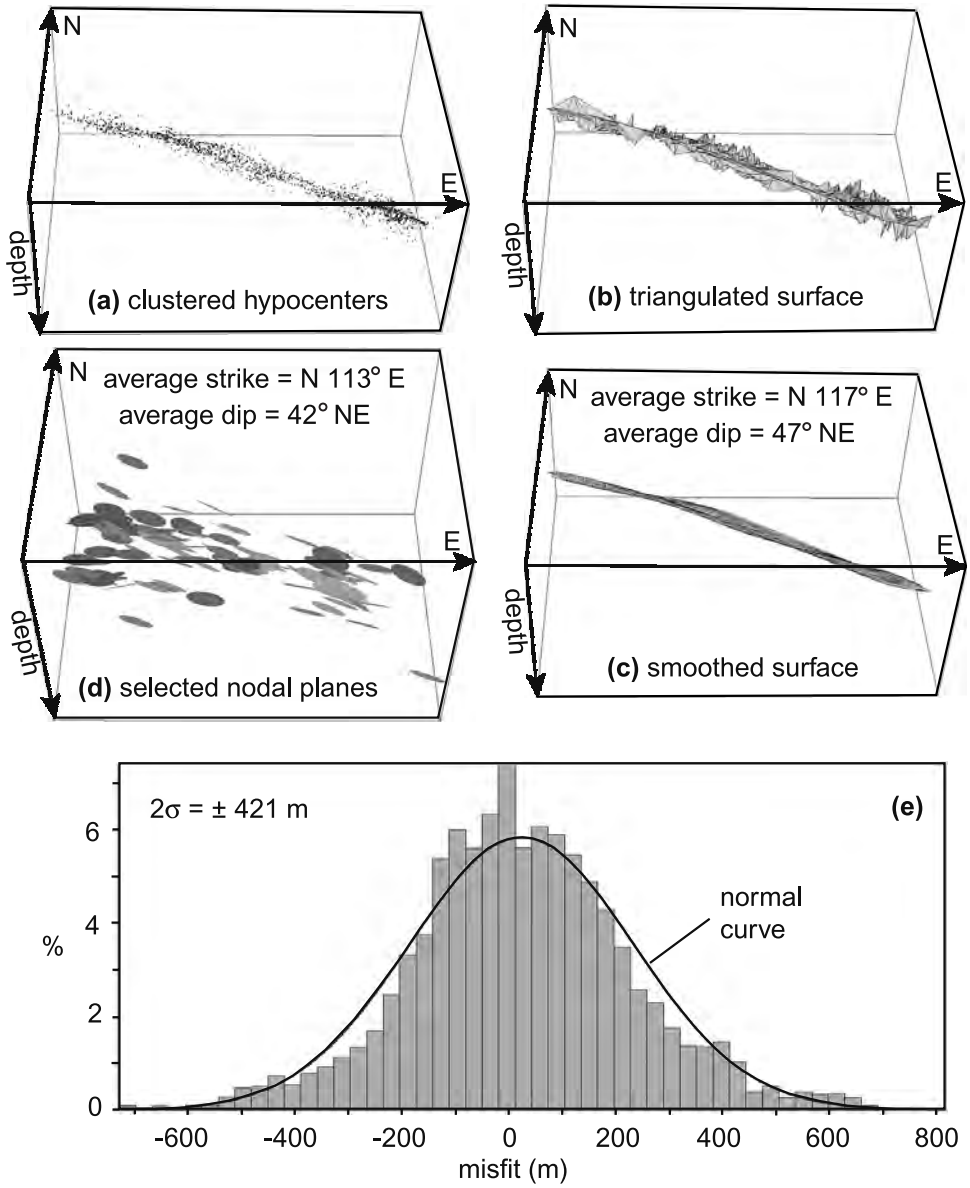

Figure 3. Steps to generate a 3-D fault surface. (a) From the clustered hypocenters (b) a triangulated surface is obtained by connecting all points. (c) The triangulated surface is then smoothed. (d) The spatial orientation of the surface can be directly compared to the earthquake focal mechanisms. (e) The histogram shows the misfit between the hypocenter cluster (Figure 3a) and the smoothed surface (Figure 3c) (negative misfit is an event on the footwall side, positive misfit is an event on the hanging wall side). Over 95% of the hypocenters fall within 421 m (2σ) of the smoothed surface. The cluster of hypocenters used here is indicated in Figure 2b and is composed by the aftershocks of the 1986 M_w 6.0 [*Stein and Hanks*, 1998], M_L 5.9 [*Jones et al.*, 1986] North Palm Springs earthquake.

projections to the Earth's surface coincide with recognized active faults, their slip azimuth is parallel in map view to the strike of these active faults (Figure 8), and their sense of slip (dextral) is consistent as well. We could therefore extend them into areas where they are not directly illuminated by earthquakes. Several of the imaged faults, some of which have sizes comparable to the 1994 Northridge earthquake rupture area (~300 km^2 [*Wald et al.*, 1996]), do not have any readily identifiable surface expression. For example, this is the case for most of the northwest trending faults visible in Figure 4b included in the area southwest of 34° and northeast of the SJFZ. We shall now discuss the 3-D geometry of the two main faults in this area: the San Gorgonio Pass thrust (SGPT) and the San Andreas Fault (SAF).

3.2.1. San Gorgonio Pass Thrust

[20] We obtained a simple geometry for the SGPT west of San Gorgonio Pass from its surface trace and the assumption that its orientation is similar to that of the patch that produced numerous aftershocks of the 1986 North Palm Springs earthquake (M_w 6.0 [*Stein and Hanks*, 1998]; M_L 5.9 [*Jones et al.*, 1986]) (Figures 2, 3, and 5), already considered part of the San Gorgonio Pass thrust zone by *Seeber and Armbruster* [1995] and by *Yule and Sieh* [2003].

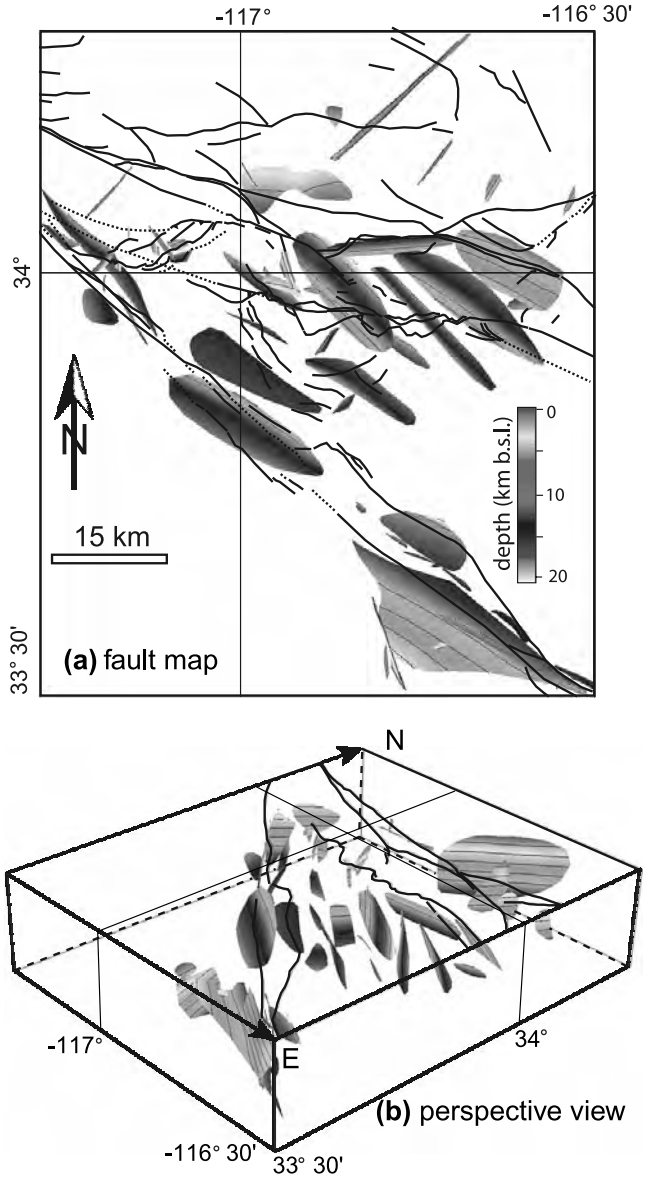

Figure 4. (a) Map and (b) view from the southeast of about 60 fault surfaces we modeled from the events shown in Figure 2. Color indicates depth, and contour spacing on faults is 3 km. See color version of this figure at back of this issue.

For this patch, the slip vector obtained from focal mechanisms (Figure 8 shows its horizontal component) indicates a combination of reverse and right-lateral strike-slip motion on the SGPT. *Yule and Sieh* [2003] consider the Banning segment of the San Andreas Fault (SAFbn) as the surface trace of the fault that ruptured in 1986. However, based on the strike, dip, and location of the 1986 patch (see also the cross sections from *Jones et al.* [1986]), having the SAFbn as the surface trace would make it necessary for the fault to steepen sharply near the surface, which would be an unusual behavior for a thrust fault. The projection of this fault patch to the surface is in fact closer to the Garnet Hill fault trace, which we therefore used as a constraint. *Bowman et al.* [2003] showed that oblique slip on a buried master fault tends to propagate as thrust faulting at shallower depths on the hanging wall side, and as strike-slip faulting directly above the tip of the propagating fault near the Earth's surface. In our model, this kind of spatial relationship exists between the SAFbn and the 1986 patch, which merge at depth (Figure 7).

[21] The thrust is segmented by three faults (F1, F2, F3 in Figures 5–7) that, as explained above, are illuminated by earthquakes only below 6–7 km depth. Focal mechanisms of these faults vary from a combination of reverse and right-lateral strike-slip motion (F3, Figure 8) similar to that of the SGPT, to nearly pure right-lateral strike slip (F1, F2). Specific information about fault size, orientation and slip of these faults is tabulated in Table 1.

3.2.2. San Andreas Fault Near San Gorgonio Pass

[22] The San Andreas Fault is not illuminated by earthquakes between Cajon Pass and Indio (Figure 2), and even its surface trace disappears between Banning and San Gorgonio Pass (Figure 1). However, we can still look to see if solutions to the fault geometry exist that allow a subvertical SAF to pass through this region [*Allen*, 1957; *Matti et al.*, 1985], at least at depths greater than 2–3 km below sea level. The absence of a clear SAF trace above the SGPT suggests that the thrust might prevent the development of a well-localized SAF rupture at shallow depth, but this does not necessarily mean that a continuous subvertical San Andreas cannot exist below the SGPT, as suggested by *Seeber and Armbruster* [1995]. Also, before it disappears, the SAF trace curves south when it encounters the western and eastern ends of the San Gorgonio Pass fault zone, suggesting that the bending could be related to the presence of the SGPT.

[23] There are two possibilities for the existence of a subvertical SAF, both illustrated in Figure 5, whereas another scenario is the absence of a vertical SAF. We model these three cases in the following sections.

3.2.2.1. Model of a Straight Connection at Depth

[24] This hypothesis has been tested by several authors, coming to different conclusions [see, e.g., *Allen*, 1957; *Seeber and Armbruster*, 1995; *Morton and Matti*, 1993; *Magistrale and Sanders*, 1996]. We model a possible straight connection between the SAFsb and the SAFbn below the SGPT (i.e., below 2.5 km depth). However, there are other faults in this area that must be taken into account. Of the faults shown in Figure 5, only F3 is positioned in such a way that an interpolated subvertical SAF would crosscut it in an unstable geometry, meaning that any slip on the SAF must offset it. An unstable fault intersection is one in which the line of intersection of two faults is not parallel to the slip direction of either fault. F3 is very well constrained by earthquakes (the quality is comparable to the 1986 North Palm Springs patch), and the intersection with a deep SAF would be strongly oblique, cutting F3 in half. F3 does not show any offset due to slip on the SAF at our current resolution (about 600 m for horizontal offsets), whereas the offset in the SGPT trace matching the surface projection of F3 is about 2 km (Figures 5 and 6), and it is consistent with the slip direction of F3 obtained from focal mechanisms (Figure 8).

[25] We do not know the age of F3, but this fault must have existed long enough to influence the geometry of the SGPT. If the SAFbn intersects F3, the offset of F3 should be clearly visible, unless F3 is very young. Probable offsets on

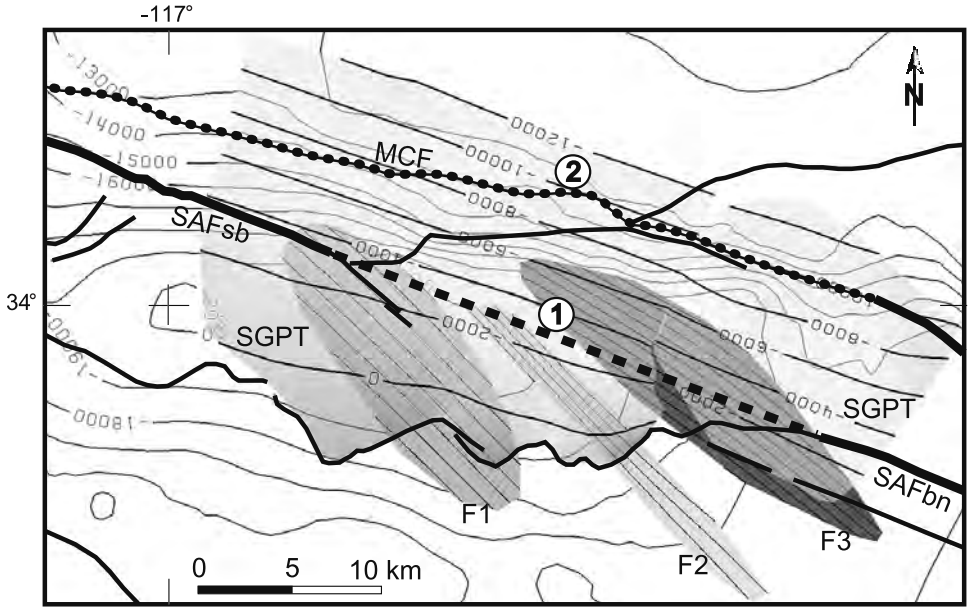

Figure 5. Map showing two possible paths for a vertical, throughgoing SAF across San Gorgonio Pass, indicated by circled numbers 1 (straight connection from SAFsb to SAFbn) and 2 (SAF follows the MCF trace). F1, F2, and F3 are faults in the footwall of the SGPT. Contour spacing on the faults is 2 km. Contour lines in the background show the depth to the base of the seismicity (contour spacing 1 km). SAFsb, San Bernardino segment of the San Andreas Fault; SAFbn, Banning segment of the San Andreas Fault; MCF, Mill Creek fault; SGPT, San Gorgonio Pass thrust.

the Yucaipa segment of the SAF (SAFsb) [*Petersen and Wesnousky*, 1994] vary between 300 m (14,000–20,000 years) and 1040 m (69,000–90,000 years), and since 125,000 years both the SAFsb and SAFbn have accumulated about 3 km of slip [*Matti et al.*, 1992]. Offsets in the upper part of this range would already be visible at our resolution; therefore, F3 would have to be younger than about 60,000 years for the offset not to be resolvable. However, unless the slip rate of F3 is at least twice that of the SAFsb and SAFbn, this is not enough time to produce a 2 km horizontal offset in the SGPT trace, especially considering that the long-term slip on F3 might not be pure strike slip.

3.2.2.2. Model of Mill Creek Connection at Depth

[26] We model a possible deep SAFsb that does not connect in a straight line to the SAFbn, but follows a more complex path. The simplest solution in this case is for the SAFcv to continue north, skirting F3 on its eastern side, and following at depth the trace of the Mill Creek fault (MCF, Figure 5), with the Mill Creek fault being effectively the old surface trace of the SAF. In fact, the MCF trace itself does not show any clear indications of Holocene activity [*Matti et al.*, 1992], which excludes the presence of a currently active vertical SAF at shallow crustal levels below it. Below the MCF trace, the SGPT reaches depths of 8–10 km, while the depth of the base of the seismicity ranges from 12 to 14 km (Figure 5). This leaves as little as 2–3 km of potentially seismogenic SAF in some stretches. Moreover, a path that follows the MCF trace has the disadvantage of a less-than-optimal fault orientation relative to the regional stress field (see below). The actual deviation from optimal orientation is even greater if we take into account the effects of reverse slip on the SGPT. We would expect some displacement to the southwest in the hanging wall of the SGPT. If an active SAF runs below the SGPT, the inactive Mill Creek trace should fall to the SW of it. However, this means the deep active fault should strike even more east-west than the Mill Creek trace. This geometrical problem exists whether the active fault is still in the seismogenic crust, or below it. On the basis of the above considerations, we therefore believe that a presently active (seismic or aseismic) SAF at any level east of the San Gorgonio Pass thrust is not a likely solution.

[27] Any path south of F3 would have to be even more complex, or the San Andreas Fault would have to be far from vertical. The latter hypothesis calls for fault dips and locations that basically coincide with those of the SGPT system.

3.2.2.3. Model of No Vertical San Andreas Fault at Depth

[28] We have so far excluded the two possible configurations for a vertical San Andreas through the region. A third possible configuration involves a nonvertical, northeast dipping San Andreas Fault through San Gorgonio Pass.

[29] On the basis of earthquake data and on the absence of a simple, well-defined surface trace (characteristic instead of the SAF everywhere else), the SAF through San Gorgonio Pass must be a complex network of fault segments rather than a simple throughgoing fault (Figure 7). The central element of this fault system would be the San Gorgonio Pass thrust (SGPT), whose geometry and slip direction we addressed earlier, together with several other faults (F1, F2, F3, see Figures 5–8, and section 3.2.1). The SGPT can connect directly with the SAFbn to the SE forming a continuous fault which steepens progressively (Figure 7), while the connection with the SAFsb to the northwest is

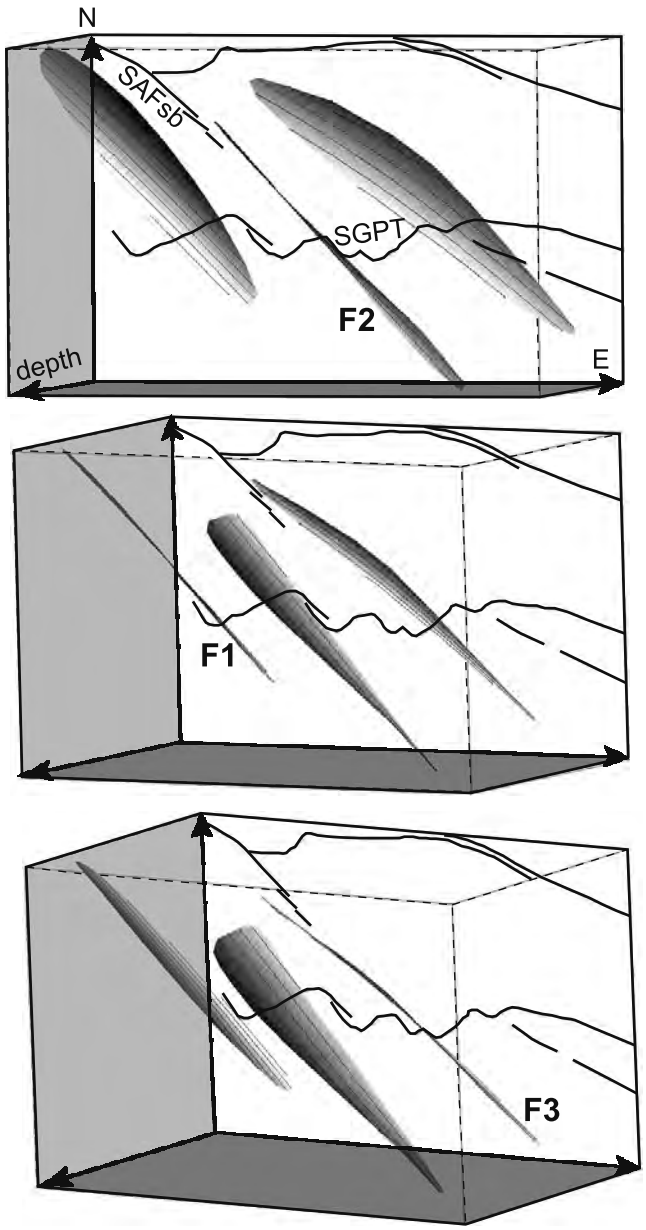

fault depths (km b.s.l.)		
	top	bottom
F1	6	20
F2	10	18
F3	7	17

Figure 6. Relationship between fault traces and geometry at depth. The three plots are aligned, from top to bottom, to give down-dip views of F2, F1, and F3, respectively. In 3-D, faults F1, F2, and F3 align with the tear faults that create steps in the trace of the SGPT. This indicates that F1, F2, and F3, though not illuminated by earthquakes at depths shallower than 6–7 km, most likely come all the way to the surface. This figure is supplemented by the ''footwall faults'' video.

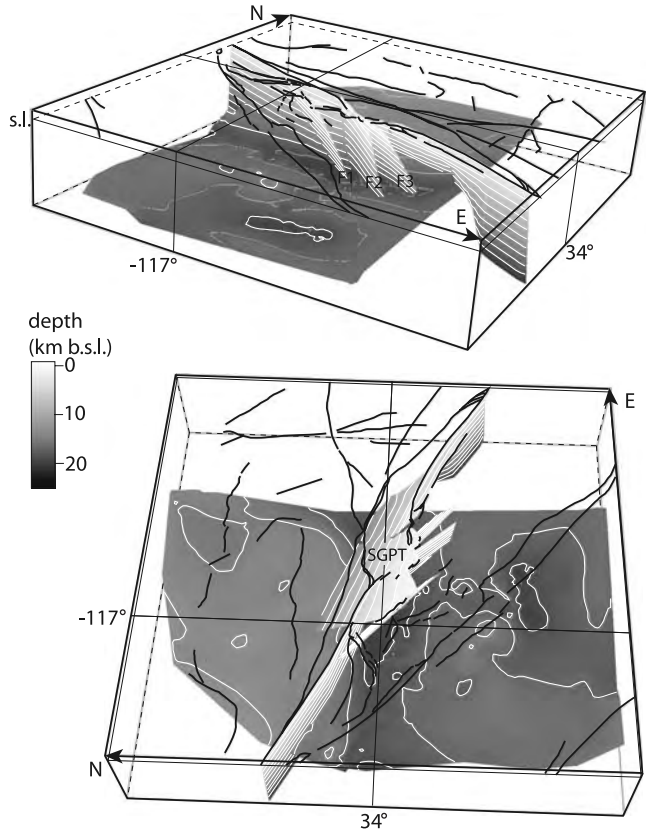

Figure 7. Two different views of the detailed 3-D geometry of the San Andreas fault system between Cajon Pass and Indio. The dark surface near the bottom of the plot represents the base of the seismicity in this area. This figure is supplemented by the ''SGP details'' video.

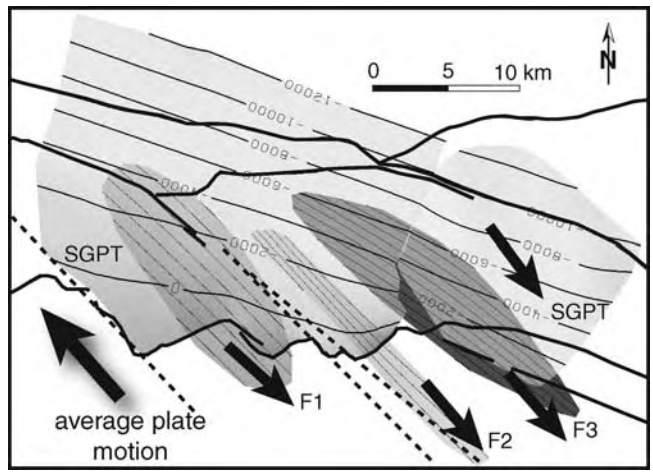

Figure 8. Southeast pointing arrows represent the horizontal component of slip direction obtained from focal mechanisms (slip direction of the hanging wall, as all faults dip to the northeast), while the northwest pointing arrow represents the horizontal component of the average motion of the San Jacinto Mountain block (delimited by the SJFZ to the west, the SAFbn/SAFcv to the east, and the SGPT to the north (see Figure 1)). The slip azimuths of all four faults are very similar, and they are nearly parallel to the average horizontal plate motion. The contour interval on the faults is 2 km. Dashed lines represent the surface projections of F1, F2, and F3.

Table 1. Fault Characteristics

Fault Name	Area, km^2	Mean Strike, deg	Mean Dip, deg	Mean Rake,[a] deg
San Gorgonio Pass thrust	839	N 111 E	41 E	140
F1	232[b]	N 134 E	65 E	−173
F2	161[b]	N 136 E	76 E	179
F3	212[b]	N 125 E	70 E	141

[a]*Aki and Richards* [1980] convention for rake (positive is reverse, negative is normal).

[b]Only area illuminated by earthquakes; does not include extension to the surface trace.

achieved by tear faults (F2 and F3, Figures 5–8) whose slip direction is compatible with that of the SGPT (Figure 8). For all practical purposes, the San Gorgonio Pass thrust is the San Andreas Fault, taking up both shortening due to the restraining step, and part of the right-lateral strike-slip component (Figure 8). More of the strike-slip component can be accommodated by a series of northeast dipping faults, three of which coincide with steps in the SGPT surface trace (more faults with similar orientation can be seen in Figure 4). In fact, the two of these faults mentioned above (F2 and F3) appear to be a natural extension of the SAFsb to the southeast (Figures 7 and 8), and are associated with magnetic anomalies at depth [*Langenheim et al.*, 2002]. Our location for the SAF is also supported by evidence of significant Holocene activity for the SAFsb, SGPT and SAFbn fault segments [e.g., *Matti et al.*, 1992; *Yule and Sieh*, 2001, 2003]. In conclusion, a northeast dipping SAF coincident with the SGPT system is our preferred solution. This solution is also similar to the geometry that *Yule and Sieh* [2003] obtained from detailed geologic mapping and from the aftershock locations of the 1986 North Palm Springs and the 1948 Desert Hot Springs earthquakes. One major difference lies in the fact that in our model the tear faults at the western end of the SGPT (F1, F2, F3) are not limited to the hanging wall of the SGPT, but extend well into the footwall, as clearly shown by earthquake hypocenter locations of regional seismicity (Figures 2, 6, and 8). Also based on earthquake locations, in our model the surface trace corresponding to the North Palm Springs aftershock cluster, and therefore the eastern SGPT, is the Garnet Hill fault trace rather than the SAFbn. The two faults however merge at depth in both models.

[30] We have so far established what is the most likely configuration of the San Andreas fault system southeast of Cajon Pass. In order to apply this result to the analysis of recent and future earthquakes, we must take into account the slip rates of these faults, and determine where most of the deformation concentrates over time. We will therefore examine both the current, measured geodetic velocities in southern California, and longer-term fault slip rates obtained from geological and paleoseismological studies.

4. Plate Boundaries and Tectonic Loading

[31] The determination of fault geometry and the spatial relationship between faults needs to be combined with additional information about their slip rates in order to study possible fault rupture sequences. An estimate of long-term tectonic loading for all the faults involved allows us to calculate how much an earthquake will move a particular fault closer or away from rupture, which we will do in the next sections. In addition, we would like to determine which are the dominant faults in the area, and in particular we would like to know whether the San Andreas is still the dominant fault, or if the San Jacinto fault system instead is the current locus of deformation. We therefore examine the plate boundary in southern California to determine which faults are accommodating most of the deformation and at what rates.

[32] If we look at the pre-Landers horizontal velocity field for southern California (Figure 9) [*Shen et al.*, 1997] (the model can be downloaded from the Southern California Earthquake Center at http://www.scec.org), the steepest velocity gradients coincide with the SAFcv-ECSZ and the SJFZ-SAF systems, indicating that here is where most of the deformation must be concentrated today. In contrast, remarkably little relative motion can currently be discerned in the velocity field between the Mojave and San Jacinto blocks (Figure 9), suggesting much lower slip rates on the SAFsb and the SGPT. This minor present motion between the San Jacinto and Mojave blocks is also seen in the optimized block model of southern California of *Meade et al.* [2002], which finds a slip rate of about 5 mm/yr for the SAFsb. A low slip rate can also be inferred from the long recurrence interval (~300 years) for earthquakes on the SAFsb segment in the last 2000 years and from slip rate on the SGPT of a few mm/yr [*Yule and Sieh*, 2001, 2003]. In sharp contrast with these observations, much larger geologic rates have been generally accepted (a well constrained 25 mm/y Holocene rate is documented at Cajon Pass by *Weldon and Sieh* [1985]; a rate of 15–25 mm/yr is commonly quoted for the eastern end of the SAFsb based on estimated soil ages of offset alluvial fans, but the uncertainties are extremely large [*Harden and Matti*, 1989]). It is beyond the scope of this paper to resolve these discrepancies in any fundamental way; we have used both rates in our modeling below. However we note that the rate of 25 mm/yr at Cajon Pass, by its location does not provide a strong constraint on the deep crustal rate of the SAFsb-SGPT, which is the prime issue in our modeling.

[33] Both the San Jacinto and San Andreas fault systems have the potential by their gross lengths to produce similarly large, destructive earthquakes, up to at least M_w 7.5. Large ruptures on one of the two systems can strongly influence the behavior of the other, as we will see later. Owing to the differences in slip rates and fault orientation, the various fault segments load differently over time, and this will influence the likelihood of a specific fault rupture sequence happening. In modeling tectonic loading (Figure 10), we followed *Hubert-Ferrari et al.* [2000], driving displacement on a dislocation by imposing steady slip below a certain locking depth, which is equivalent to long-term surface slip. Our goal is to match the horizontal velocity field in southern California [*Shen et al.*, 1997] as closely as possible.

[34] We used published fault slip rates from various sources [*Weldon and Sieh*, 1985; *Harden and Matti*, 1989; *Morton and Matti*, 1993; *Dorsey*, 2004; *Meade et al.*, 2002], the inset in Figure 10 shows the combination of slip rates that best matches the observed velocity field when the following locking depths are used: 10 km for the ECSZ

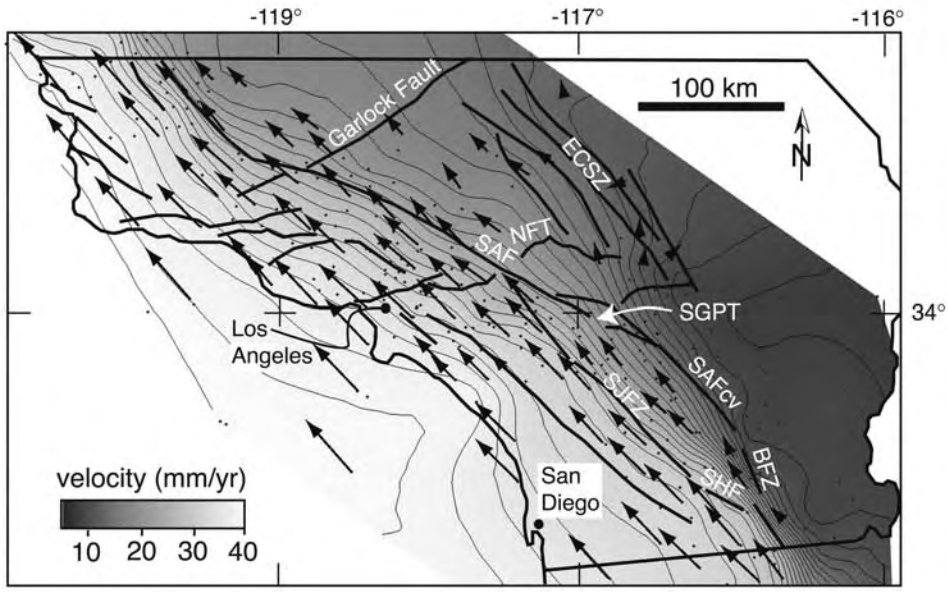

Figure 9. Velocity map derived from the Crustal Deformation Velocity Map of Southern California V. 2.0 [*Shen et al.*, 1997] (the model can be downloaded from the Southern California Earthquake Center at http://www.scec.org). We used only pre-Landers velocities, plotted with respect to the North American plate. For clarity, not all vectors have been plotted. Dots represent stations. The velocity contours (based on magnitude of the velocity vectors; spacing is about 2 mm/yr) show that the highest velocity gradients coincide with the SAF and the ECSZ north of Los Angeles, and with the SAF and the SJFZ south of it. There is no clear evidence of relative motion across the SGPT, as the difference in average velocity between the Mojave desert to the north and the San Jacinto Mountain block to the south is smaller than the uncertainty in the velocity vectors. The Mojave block is here delimited by the SAF to the west, the ECSZ to the east, the Garlock fault to the north and the North Frontal thrust (NFT) to the south. The San Jacinto block is delimited by the SJFZ to the west, the SAFcv to the east, the SAFsb-SGPT to the north, and the Brawley seismic zone (BSZ) and the Superstition Hill fault (SHF) to the south. The SGPT is dipping 41° to the northeast in our model (see Table 1); all the others are vertical boundaries.

(based on the depth to the bottom of the seismogenic crust in the Mojave block) and the faults just south of SJFZ and SAFcv, (also based on shallower seismicity), and 15 km for the remaining fault segments. In particular, present-day slip rates higher than about 5 mm/yr on the SAFsb-SGPT segments produce poor matches to the velocity field. This suggests that today the main boundary in the region is not presently the ''classic'' San Andreas system (Coachella Valley-San Bernardino-Mojave), but rather deformation is equally split between the SAF-SJFZ, which constitute one system, and the ECSZ-SAFcv, which form the other. In this view the SAFsb-SGPT would still be active, but accommodating only a minor fraction of the deformation.

[35] Some of the residuals still visible in Figure 10 (most of them below 1 mm/yr) are due to the simplified fault geometry we used. There is a systematically increasing slip deficit west of the SAF-SJFZ, and the residuals at some stations east of it are abnormally high. In fact, we did not model the contributions from the western Transverse Ranges and from the faults west of the SJFZ (Elsinore fault, Newport-Inglewood fault zone, Palos Verdes-Coronado Bank fault zone, San Clemente fault zone), and this accounts for the increase in slip deficit from east to west. In addition, we modeled the ECSZ as a single boundary approximately following the Landers rupture zone, instead of a set of subparallel faults, which accounts for the fact that some stations show anomalous residuals even as stations close by display almost no residuals at all.

5. Earthquake Triggering Scenarios

[36] The second of our two initial questions was if a throughgoing rupture of the San Andreas Fault through the San Gorgonio Pass region is possible. On the basis of the results from our 3-D fault modeling in this region (Figures 3–8) and on the considerations outlined in the section above, we explored four simple earthquake scenarios (Figures 11–15) to examine possible fault interactions and to determine the most favorable conditions, if any exist, for a hypothetical throughgoing rupture of the SAF system from the Mojave Desert to Coachella Valley. These are worst case scenarios, where the faults are allowed to rupture all the way from the surface to the base of the seismogenic zone. We calculated the static change in the Coulomb stress state for each scenario following *King et al.* [1994], *Toda et al.* [1998], *Hubert-Ferrari et al.* [2000], and *Toda and Stein* [2002] using the software Coulomb developed by *Toda et al.* [1998] and *Toda and Stein* [2002] available at http://quake.wr.usgs.gov/research/deformation/modeling/coulomb.

[37] Besides the geometry and slip parameters of the various faults involved, this type of modeling requires the

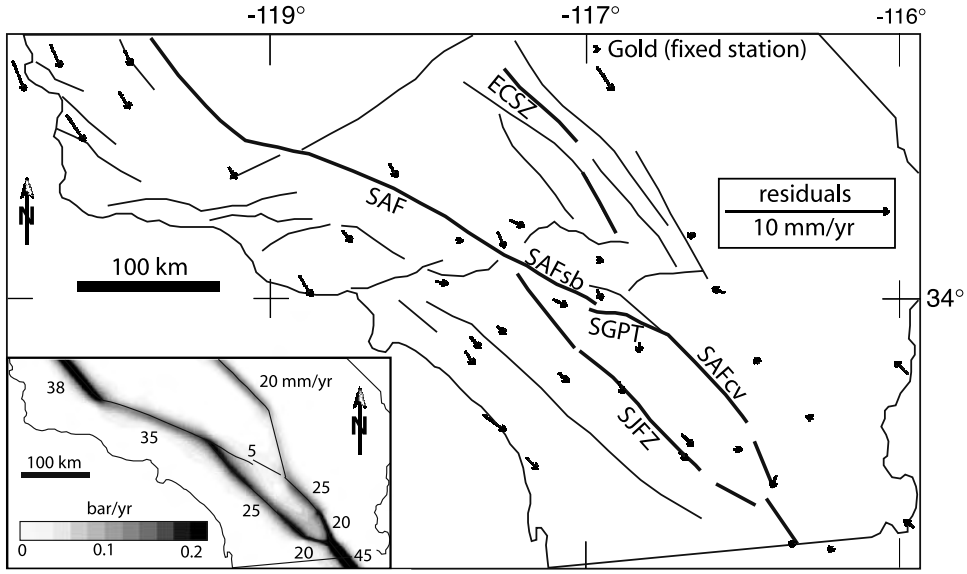

Figure 10. Tectonic loading model. Arrows indicate residuals obtained by subtracting the modeled displacements from those of the Crustal Deformation Velocity Map of Southern California V2.0 [*Shen et al.*, 1997] (the model can be downloaded from the Southern California Earthquake Center at http://www.scec.org), at 36 randomly selected stations. Residuals are calculated keeping the station "Gold" as fixed reference station. The range of values is 0–2 mm/yr, with most residuals below 1 mm/yr. Inset shows the fault segments used in the calculation and the stress loading at 6 km depth (which is the depth of plots in Figures 11, 13, and 14); numbers indicate the slip rates (mm/yr) we used for each segment (see text for further discussion and references to published rates). Loading in the area around SAFsb and SGPT is below 0.04 bar/yr, less than half the minimum load on the remaining segments of the SAF system. The model shown here, as well as the models shown in Figures 11 and 13–15, is available as supplementary data. SAF, San Andreas Fault north of Cajon Pass; SAFsb, San Bernardino segment of the SAF; SAFcv, Coachella Valley segment of the SAF; ECSZ, eastern California shear zone; SGPT, San Gorgonio Pass thrust.

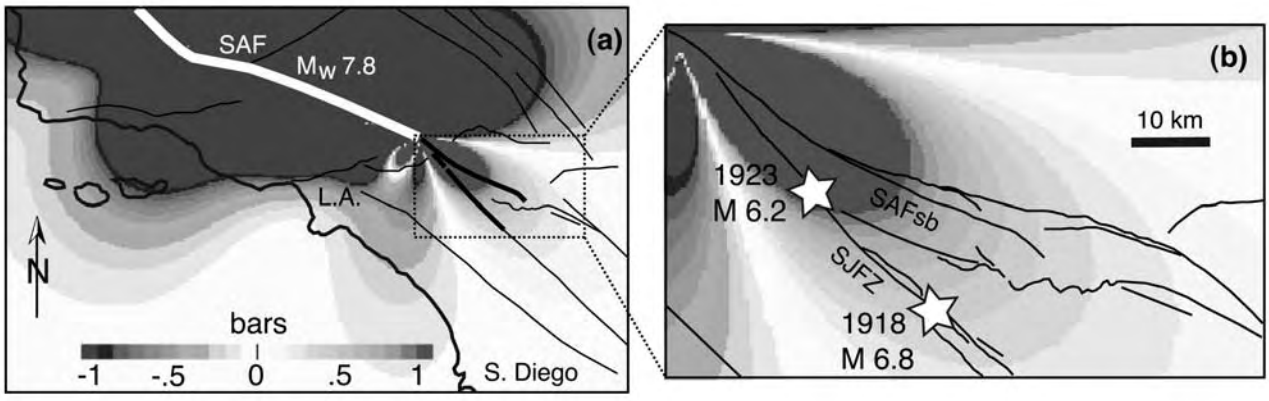

Figure 11. "Fort Tejon" earthquake scenario. (a) Coulomb stress changes caused by a hypothetical rupture of the San Andreas Fault north of Cajon Pass (SAF) in an event like the 1857 great Fort Tejon earthquake. (b) The effects are calculated on the San Jacinto fault zone (SJFZ) and the San Bernardino segment of the San Andreas Fault (SAFsb). This event would cause a stress increase >0.4 bars on the SAFsb and most of the SJFZ. Following the 1857 event, two earthquakes occurred on the SJFZ in 1918 and 1923. For this figure and all subsequent ones, calculation depth = 6 km, coefficient of friction = 0.4. See color version of this figure at back of this issue.

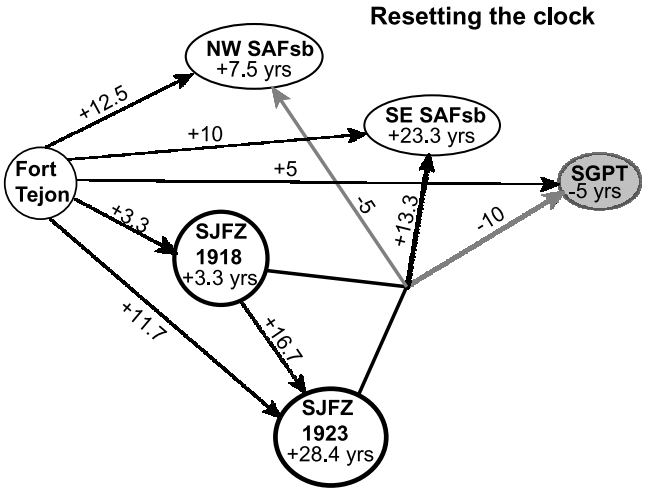

Figure 12. Diagram that illustrates how an earthquake can "reset the clock" by delaying or advancing the occurrence of future events on nearby faults. Here we see the effect of the 1857 Fort Tejon earthquake and the combined effect of the 1918 and 1923 SJFZ earthquakes. The numbers next to each arrow represent the years by which rupture of a certain fault segment has been advanced (+, black) or delayed (−, gray). In other words, they are the equivalent number of years of tectonic loading for a given fault. The total clock advancement or delay is indicated inside each circle. SJFZ, San Jacinto fault zone; SAFsb, San Bernardino segment of the San Andreas Fault; SGPT, San Gorgonio Pass thrust.

knowledge of two other parameters: coefficient of friction and regional stress field [*King et al.*, 1994]. The coefficient of friction mainly influences the magnitude of the Coulomb stress change rather than the overall pattern. Most authors have considered that friction on the San Andreas Fault itself could be as low as 0.25 or even less, based on a low heat flow and stress rotations near the fault [e.g., *Lachenbruch and Sass*, 1992; *Hardebeck and Hauksson*, 2001; *Townend and Zoback*, 2001], but friction as high as 0.6–0.7 have also been proposed by *Scholz* [2000]. *King et al.* [1994] assumed 0.4 as coefficient of friction when studying the Landers earthquake sequence, showing that their calculations are only moderately sensitive to friction values, where they consider reasonable values between 0 and 0.75. On the basis of their observations, we also chose a this relatively conservative coefficient of friction of 0.4 for our calculations, after verifying that a higher or lower value did not produce any fundamental changes in our results.

[38] Rather than calculating Coulomb stress changes for optimal fault orientations, which is a common strategy, we applied the calculations to specific faults for which we know the 3-D geometry reasonably well. As these are all major, well-developed faults, it is logical to assume that the likelihood of any of them rupturing in the future in a large earthquake is much higher than for an entirely new major fault to be created. In addition, calculating the Coulomb stress changes for known faults does not require knowledge of the regional stress field [*King et al.*, 1994]. All the calculations shown in Figures 11–15 are plotted at a depth

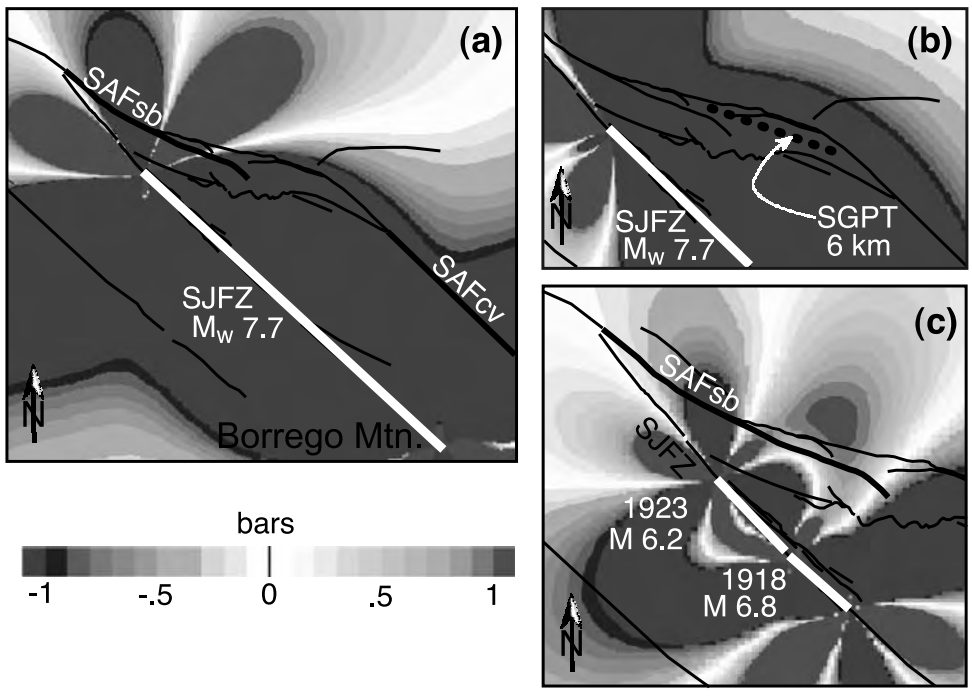

Figure 13. "San Jacinto" earthquake scenario. Coulomb stress changes caused by a hypothetical M_w 7.7 earthquake on the San Jacinto fault zone (SJFZ), calculated (a) on San Bernardino segment of the San Andreas Fault (SAFsb) and on the Coachella valley segment of the San Andreas Fault (SAFcv) and (b) on the San Gorgonio Pass thrust (SGPT). Stress is greatly decreased on the SAFcv and the SGPT, while both positive and negative changes affect the SAFsb. (c) Smaller earthquakes on the northern part of SJFZ have a similar effect on the SAFsb. Events on SJFZ thus tend to inhibit ruptures of the SAF system south of Cajon Pass. See color version of this figure at back of this issue.

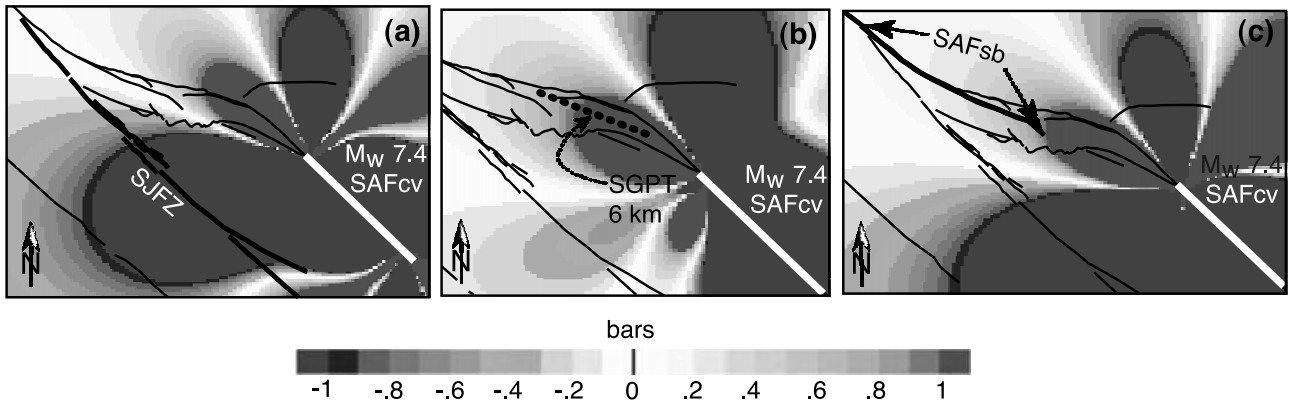

Figure 14. "Coachella" earthquake scenario. Coulomb stress changes caused by a hypothetical M_w 7.4 earthquake on the Coachella valley segment of the San Andreas Fault (SAFcv), calculated (a) on the San Jacinto fault zone (SJFZ), (b) on the San Gorgonio Pass thrust (SGPT), and (c) on the San Bernardino segment of the San Andreas Fault (SAFsb). While an event on the SAFcv would inhibit rupture on the SJFZ, it would at the same time bring the entire San Gorgonio Pass stepover (SAFbn + SGPT + SAFsb) closer to failure. See color version of this figure at back of this issue.

of 6 km. Below we describe the four earthquake scenarios, which we labeled "Fort Tejon", "San Jacinto", "Coachella", and "San Bernardino-San Gorgonio" based on the fault segments that rupture in each scenario.

5.1. "Fort Tejon" Rupture Scenario

[39] The great 1857 Fort Tejon earthquake is an actual example of a major rupture of the SAF north of Cajon Pass, which we can use as our first scenario to determine what effects a similar event would produce on the SJFZ and the SAFsb (Figure 11). This earthquake ruptured the SAF in a 360-km-long stretch from Parkfield to Cajon Pass [*Sieh*, 1978]. *Sanders* [1993], based on the earthquakes migration pattern, related this event to the triggering of a 90 years long earthquake sequence on the SJFZ, and showed that the Mojave segment of the SAF and the SJFZ trigger each other. We want to explore this possibility further, and extend it to include the interactions with all the other segments in the SAF system.

[40] In order to calculate the Coulomb stress changes due to this earthquake, we used the slip distribution modeled by *Harris and Simpson* [1996], with a fault rupture extending from the surface to 15 km depth. This choice of parameters results in an M_w 7.8 event. We calculated the Coulomb stress changes specifically on the SJFZ and on the SAFsb. Figure 11 shows the Coulomb stress field for the orientation of the SAFsb. The stress field changes only slightly when calculated for the SJFZ orientation, without causing any substantial changes in terms of which faults are loaded and by how much, therefore we can consider Figure 11 representative of both faults.

[41] Looking at the effects of a Fort Tejon rupture on the SAFsb segment and the SJFZ system, we see that both experience a Coulomb stress increase, moving closer to failure. The increase corresponds on average to 10 years of tectonic loading for the SAFsb and 7–8 years of tectonic loading for the SJFZ north of Anza. It is worth noticing that after the 1857 Fort Tejon earthquake, no major event occurred on the SAFsb, but 2 events with M > 6 occurred on the northern SJFZ in 1918 and 1923, indicating that the SJFZ was already closer to failure than the SAFsb. A more detailed view of how the various earthquakes on these faults "reset the clock" (that is, how many years an earthquake is delayed or advanced by the changes in static Coulomb stress produced by previous events) is shown in Figure 12. In particular, in our model the occurrence of the 1923 earthquake on the SJFZ was advanced by nearly 30 years by the combined effects of the Fort Tejon and the 1918 SJFZ events. The SAFsb has not produced any major ruptures for at least 200 years, and probably neither a complete rupture of the entire SAFsb segment nor propagation of rupture to the SGPT has occurred during the past 470 years [*Yule and Sieh*, 2001]. We will see below how the occurrence of earthquakes on the northern SJFZ and the absence of significant activity on the SAFsb segment might be related.

5.2. "San Jacinto" Rupture Scenario

[42] We examined two possible scenarios: a rupture of the entire SJFZ from San Bernardino to just south of Borrego Mtn., and smaller ruptures of the northern SJFZ between San Bernardino and Anza. Figure 13 shows the consequences of an M_w 7.7 earthquake involving the entire SJFZ south of San Bernardino. Such an event would lower the Coulomb stress by 3 bars on the SAFcv (equivalent to delaying the next rupture by about 20 years, Figure 13a) and by 2 bars on the SGPT (equivalent to delaying the next rupture by 100 years, Figure 13b). The effect on the SAFsb is less dramatic, but most of the fault will experience a Coulomb stress reduction of about 2 bars, with a small stretch somewhere in the middle subject to a Coulomb stress increase of the same magnitude. The location and length of the loaded stretch depends on where exactly the northern termination of the SJFZ rupture is located, but even in the best case (Figure 13a) only 1/4 of the SAFsb at most will be loaded, while the rest will fall into the stress shadow. This means a rupture on the SAFsb would probably be stopped before escalating into a large event.

[43] However, there are no records so far of a rupture of the entire SJFZ system (our worst case scenario), therefore we examined also situations closer to what the fault has

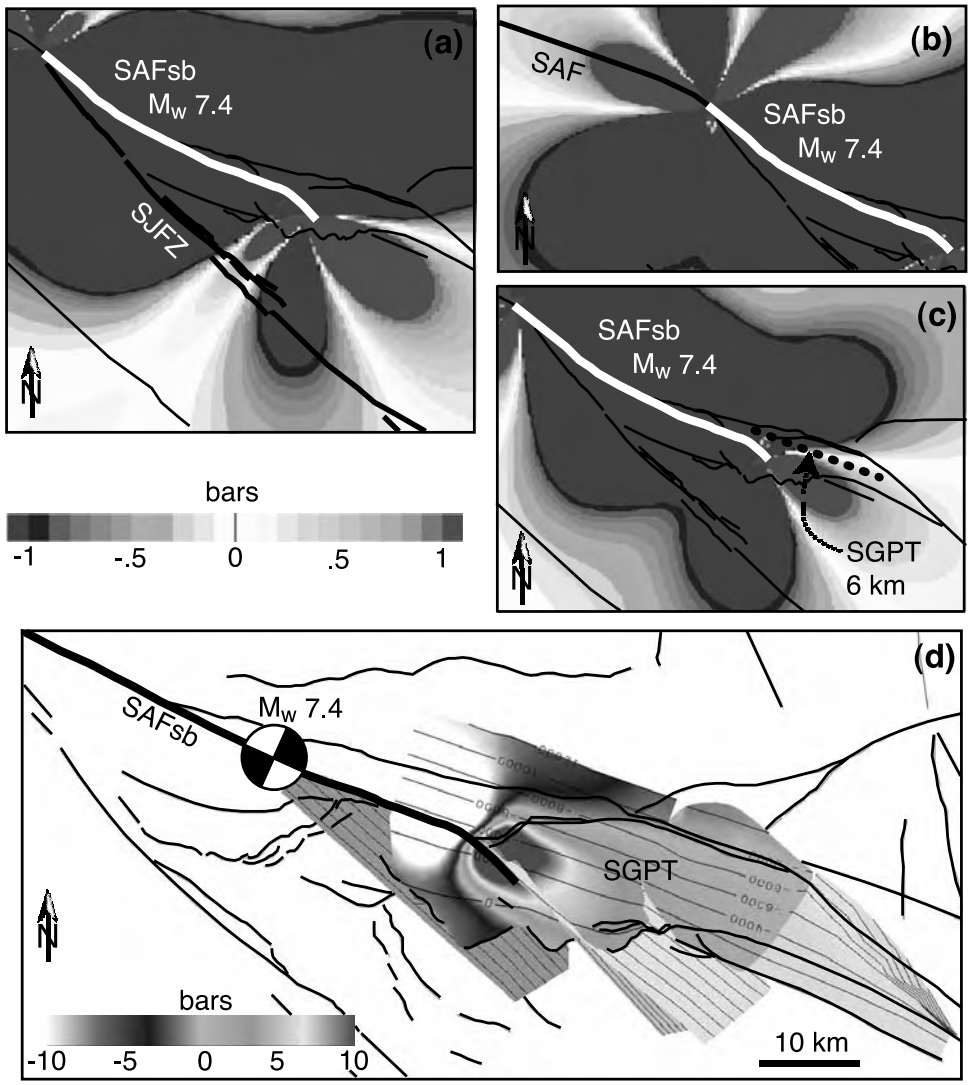

Figure 15. "San Bernardino-San Gorgonio" earthquake scenario. Coulomb stress changes caused by a hypothetical M_w 7.4 earthquake on the San Bernardino segment of the San Andreas Fault (SAFsb), calculated (a) on the San Jacinto fault zone (SJFZ), (b) on the Mojave segment of the San Andreas (SAF), and (c, d) on the San Gorgonio Pass thrust (SGPT). Figure 15d shows the coulomb stress change on the SGPT in 3-D, plotted on the fault surface itself. In this scenario the SAF northwest of Cajon Pass and the SGPT would be moved closer to failure, while ruptures on the SJFZ would be mostly inhibited. See color version of this figure at back of this issue.

recently experienced. If we consider intermediate-size events on the northern SJFZ, like those that occurred in 1918 and 1923 (Figure 13c), we see a pattern in the stress field similar to the one described above. In this case, a longer stretch of the SAFsb can be loaded, but a significant stress drop will at the same time move the SGPT and the northwestern half of the SAFsb away from failure ("erasing" 10 years and 5 years of tectonic loading respectively, see Figure 12). Thus activity on the SJFZ has the potential for controlling both size and frequency of ruptures of the SAFsb. In fact, since large earthquakes (or a series of intermediate ones) on the SJFZ tend to place most of the SAFsb-SGPT-SAFcv system in stress shadow, we would expect that a period of high level of activity of the SJFZ should coincide with a relatively quiet period for the SAF southeast of Cajon Pass in general. Activity on the SJFZ should therefore inhibit a throughgoing rupture of the SAF from the Mojave Desert to Coachella Valley.

5.3. "Coachella" Rupture Scenario

[44] A complete rupture of the SAFcv from Indio to Bombay Beach could easily produce an M_w 7.4 earthquake (Figure 14). A major event occurring on the SAFcv would result in a dramatic negative Coulomb stress change for over 90% of the SJFZ (Figure 14a) equivalent to delaying the next rupture by about 12 years. At the same time, a large earthquake on the SAFcv would significantly increase the Coulomb stress on the entire SGPT (Figure 14b), bringing it closer to rupture by 65 years, and directly load the SAFsb as well (Figure 14c), albeit to a lesser degree (the clock is moved forward only by 2 to 4 years). A rupture initiation on the SAFcv is

probably the best scenario for both a throughgoing SAF rupture to the Mojave Desert, and for a general increase in earthquake activity of the SGPT-SAFsb system. It would shut off most of the activity on the SJFZ that, as explained above, would otherwise tend to change the stress field unfavorably with respect to SGPT-SAFsb ruptures. In fact, the spacing (~40 km) between the SJFZ and SAFcv is such that events above a threshold $M_w \sim 7$ on one of the two fault systems will significantly lower stress on the other, thus delaying the next rupture. This behavior is consistent with the concept of characteristic fault spacing, as discussed by *Roy and Royden* [2000], who speculate that layered crustal rheology controls this characteristic spacing.

5.4. "San Bernardino-San Gorgonio" Rupture Scenario

[45] We calculated the Coulomb stress change due to an M_w 7.4 earthquake on the SAFsb (Figure 15), produced by a rupture from 0 to 15 km depth with 3 m of right-lateral slip on average. We based the estimate of a 15 km deep fault rupture on the local average depth to the base of the seismicity directly below the SAFsb trace (12 km at the northwestern end of the fault, and 17 km at the southeastern end, Figure 5). If the slip rates along this segment are indeed in the order of 5 ± 2 mm/yr [*Meade et al.*, 2002], it should take about 600 years to accumulate a potential slip of 3 m. *Yule and Sieh* [2001] have determined an average recurrence interval of about 330 years for intermediate to large earthquakes on this segment based on paleoseismological evidence, so we would expect an average slip of 1.5 m in a single large earthquake. Our choice of 3 m of slip is meant to be conservative, because the interval of 330 years is just an average, while specific intervals can be much shorter or longer [*Yule and Sieh*, 2001], and because it could be that the current base of the seismicity does not accurately reflect the maximum depth of a future large rupture. We therefore believe that an M_w 7.4 is the largest event we can reasonably expect on this segment.

[46] The SJFZ would mostly fall into the stress shadow of such an earthquake (Figure 15a) and a potential rupture would be delayed by about 10 years. The Mojave segment of the SAF just northwest of Cajon Pass would experience a stress increase $\geq$1 bar (Figure 15b), equivalent to at least 7 years of tectonic loading. About 50% of the SGPT would also experience a stress increase $\geq$0.3 bars (Figures 15b and 15c), equivalent to at least 15 years of tectonic loading. An M_w 7.4 event however is not large enough to load the SAFcv south of Indio directly. In theory, this type of earthquake could set off a chain of ruptures to the northwest and southeast, although questions remain as to how effectively a rupture could propagate to the SGPT segment. In 3-D, the Coulomb stress change on the SGPT is not uniformly positive following a complete rupture of the SAFsb, and a shorter rupture of the SAFsb, which would create a more favorable stress pattern for slip on the SGPT, would also result in a smaller earthquake, reducing the actual stress increase at both ends of the SAFsb. Interestingly, F2 and F3 (Figure 15d) are much better oriented in terms of their rupture being encouraged by a SAFsb event. The earthquake in Figure 15 would move the clock forward by a minimum of 67 years for F2, and by 53 years for F1. These faults are also optimally oriented in terms of tectonic loading, more so than the SGPT (they load faster, about 0.03 bar/yr against 0.02 bar/yr).

[47] An intermediate-size rupture of the SGPT system is probably not enough to set off a chain of ruptures involving the SAFsb and SAFcv under normal circumstances (i.e., unless the other faults are basically at failure already). The SGPT-SAFbn system ruptured twice in the last 55 years, first in the 1948, M_w 6.0 [*Nicholson*, 1996] Desert Hot Springs earthquake, and then in the 1986, M_w 6.0 [*Stein and Hanks*, 1998], M_L 5.9 [*Jones et al.*, 1986] North Palm Springs earthquake. These events did not trigger any earthquakes of comparable size or larger on nearby faults immediately after, even though both the SAFsb and the SAFcv are optimally oriented and experienced a small increase in Coulomb stress. The Desert Hot Springs earthquake did however move the clock forward for the North Palm Springs segment by about 12 years, counteracting the stress shadow of the combined 1918–1923 SJFZ events.

6. Discussion and Conclusions

[48] The San Andreas Fault is a localized, continuous fault for most of its 1200 km length. The most notable exception is the contractional stepover between Cajon Pass and Indio. We have explored this lack of continuity by mapping over 60 fault segments in this region from hypocenter locations and focal mechanisms. We have shown that knowing the position and geometry of smaller faults with relatively low slip rates can be very helpful in constraining the location and geometry of large strike-slip faults in areas where the latter are currently aseismic, because the geometry of the strike-slip fault must be compatible with the geometry, location, and slip direction on the smaller faults. Mapping the seismically illuminated faults places strong constraints on the location, geometry, and possible segmentation of the San Andreas Fault. We came to the conclusion that no throughgoing vertical active San Andreas Fault exists near San Gorgonio Pass, but rather a complex 3-D fault network with a central role played by the San Gorgonio Pass thrust. If we consider ruptures of the entire San Andreas fault system between Cajon Pass and Indio, only complex ruptures would be possible, involving a combination of right-lateral strike-slip and reverse motion.

[49] The likelihood of a throughgoing complex rupture of the San Andreas fault system from the Mojave Desert to Coachella Valley depends on interactions among nearby fault systems and on long-term tectonic loading of the San Gorgonio Pass stepover. A throughgoing rupture is theoretically possible, but we believe it is an improbable and hence infrequent event because its occurrence depends on a series of factors that have to be in the right combination at the right time: (1) the northern San Jacinto fault zone must be in a period of low activity, otherwise it would reduce Coulomb stress on parts of the San Bernardino segment of the San Andreas Fault and on the San Gorgonio Pass thrust; (2) a large earthquake ($M_w \geq 7.4$) must occur on the Mojave segment of the San Andreas Fault just north of Cajon Pass, on the San Bernardino segment, or on the Coachella Valley segment in order to increase stress adequately on the adjacent segments; (3) the San Bernardino segment and

the San Gorgonio Pass thrust must be already close enough to failure that any further increase in stress can make them fail in the appropriate sequence, otherwise the segmentation of the western end of the SGPT might stop the propagation of ruptures initiated on the San Bernardino segment. The faults segmenting the thrust are better oriented for failure than the thrust itself, and continue for a few km south of the thrust, at least in its footwall. If loading of the SGPT is not enough, a rupture might just involve these tear faults only, possibly rupturing new patches to the south, instead of jumping over to the SGPT. As the San Gorgonio Pass stepover loads at a lower rate than the rest of the San Andreas Fault, the third condition can be likely satisfied only when no intermediate ruptures occur on these faults for a long period of time, allowing stress to accumulate on the fault. Interestingly, about 475 years, a longer-than-average interval, have passed since the last intermediate/large earthquake occurred on the San Bernardino segment near San Gorgonio Pass, and this segment could be ready for an event large enough to jump across the San Gorgonio Pass stepover [*Yule and Sieh*, 2001].

[50] **Acknowledgments.** We thank Robert Simpson and an anonymous reviewer for thoughtful reviews. Research was supported by the U.S. Geological Survey (USGS), Department of the Interior, under USGS awards 01HQGR0028 and 02HQGR0033. The views and conclusions contained in this document are those of the authors and should not be interpreted as necessarily representing the official policies, either expressed or implied, of the U.S. Government.

References

Aki, K., and P. G. Richards (1980), *Quantitative Seismology, Theory and Methods*, W. H. Freeman, New York.

Allen, C. R. (1957), San Andreas fault zone in San Gorgonio Pass, southern California, *Geol. Soc. Am. Bull.*, *68*, 315–350.

Bowman, D. D., G. C. King, and P. Tapponnier (2003), Slip partitioning by elastoplastic propagation of oblique slip at depth, *Science*, *300*, 1121–1123.

Carena, S., and J. Suppe (2002), Three-dimensional imaging of active structures using earthquake aftershocks: The Northridge thrust, California, *J. Struct. Geol.*, *24*, 887–904.

Carena, S., J. Suppe, and H. Kao (2002), Active detachment of Taiwan illuminated by small earthquakes and its control of first-order topography, *Geology*, *30*, 935–938.

Delaunay, B. N. (1934), Sur la sphere vide, *Bull. Acad. Sci. USSR*, *VII*, 793–800.

Dickinson, W. R. (1996), Kinematics of transrotational tectonism in the California Transverse ranges and its contribution to cumulative slip along the San Andreas transform fault system, *Spec. Pap. Geol. Soc. Am.*, *305*, 46 pp.

Dorsey, R. J. (2004), Stratigraphic record of Pleistocene initiation and slip on the Coyote Creek fault, lower Coyote Creek, southern California, *Spec. Pap. Geol. Soc. Am.*, *365*, in press.

Hardebeck, J. L., and E. Hauksson (2001), Crustal stress field in southern California and its implications for fault mechanics, *J. Geophys. Res.*, *106*, 21,859–21,882.

Harden, J. W., and J. C. Matti (1989), Holocene and late Pleistocene slip rates on the San Andreas fault in Yucaipa, California, using displaced alluvial-fan deposits and soil chronology, *Geol. Soc. Am. Bull.*, *101*, 1107–1117.

Harris, R. A., and R. W. Simpson (1996), In the shadow of 1857: The effect of the great Fort Tejon earthquake on subsequent earthquakes in southern California, *Geophys. Res. Lett.*, *23*(3), 229–232.

Hauksson, E. (2000), Crustal structure and seismicity distribution adjacent to the Pacific and North America plate boundary in southern California, *J. Geophys. Res.*, *105*, 13,875–13,903.

Hubert-Ferrari, A., A. Barka, E. Jacques, S. Nalbant, B. Meyer, R. Armijo, P. Tapponnier, and G. C. P. King (2000), Seismic hazard in the Sea of Marmara following the Izmit earthquake, *Nature*, *404*, 269–273.

Jennings, C. W. (1994), Fault activity map of California and adjacent areas with location and ages of recent volcanic eruptions, *Calif. Geol. Data Map Ser., Map 6*, Calif. Div. of Mines and Geol., Sacramento.

Jones, R. H., and R. C. Stewart (1997), A method for determining significant structures in a cloud of earthquakes, *J. Geophys. Res.*, *102*, 8245–8254.

Jones, L. M., L. K. Hutton, D. D. Given, and C. R. Allen (1986), The North Palm Springs, California, earthquake sequence of July 1986, *Bull. Seismol. Soc. Am.*, *76*, 1830–1837.

King, G. C. P., R. S. Stein, and J. Lin (1994), Static stress changes and the triggering of earthquakes, *Bull. Seismol. Soc. Am.*, *84*, 935–953.

Lachenbruch, A. H., and J. H. Sass (1992), Heat flow from Cajon Pass, fault strength, and tectonic implications, *J. Geophys. Res.*, *97*, 4995–5030.

Langenheim, V. E., R. C. Jachens, J. C. Matti, D. M. Morton, and A. H. Christensen (2002), Structure of the San Gorgonio Pass region, southern California, based on analysis of gravity and magnetic data, paper 57-10 presented at the Annual Meeting, Geol. Soc. of Am., Denver, Colo.

Magistrale, H., and C. Sanders (1996), Evidence from precise earthquake hypocenters for segmentation of the San Andreas fault in San Gorgonio Pass, *J. Geophys. Res.*, *101*, 3031–3044.

Mallet, J. L. (1992), Discrete smooth interpolation in geometric modeling, *Comput. Aided Design*, *24*, 178–191.

Mallet, J. L. (2002), *Geomodeling*, Oxford Univ. Press, New York.

Matti, J. C., D. M. Morton, and B. F. Cox (1985), Distribution and geologic relations of fault systems in the vicinity of the central Transverse Ranges, southern California, scale 1:250,000, *U.S. Geol. Surv. Open File Rep., 85-365*.

Matti, J. C., D. M. Morton, and B. F. Cox (1992), The San Andreas fault system in the vicinity of the central Transverse Ranges province, southern California, *U.S. Geol. Surv. Open File Rep., 92-354*, 40 pp.

Meade, B., B. Hager, and R. King (2002), Block models of present day deformation in southern California constrained by geodetic measurements, *Eos Trans. AGU*, *83*(47), Fall Meet. Suppl., Abstract T62F-05.

Morton, D. M., and J. C. Matti (1993), Extension and contraction within an evolving divergent strike-slip fault complex: The San Andreas and San Jacinto fault zones at their convergence in southern California, *Geol. Soc. Am. Mem.*, *178*, 217–230.

Nicholson, C. (1996), Seismic behavior of the southern San Andreas fault zone in the northern Coachella Valley, California: Comparison of the 1948 and 1986 earthquake sequences, *Bull. Seismol. Soc. Am.*, *86*, 1331–1349.

Nicholson, T., M. Sambridge, and O. Gudmundsson (2000), On entropy and clustering in earthquake hypocentre distributions, *Geophys. J. Int.*, *142*, 37–51.

Oskin, M. E., J. Stock, and A. Martín-Barajas (2001), Rapid localization of Pacific-North America plate motion in the Gulf of California, *Geology*, *29*, 459–462.

Petersen, M. D., and S. G. Wesnousky (1994), Fault slip rates and earthquake histories for active faults in southern California, *Seismol. Soc. Am. Bull.*, *84*, 1608–1649.

Richards-Dinger, K., and P. M. Shearer (2000), Earthquake locations in southern California obtained using source-specific station terms, *J. Geophys. Res.*, *105*, 10,939–10,960.

Roy, M., and L. H. Royden (2000), Crustal rheology and faulting at strike-slip plate boundaries: 2. Effects of lower crustal flow, *J. Geophys. Res.*, *105*, 5599–5613.

Sanders, C. O. (1993), Interaction of the San Jacinto and San Andreas fault zones, southern California: Triggered earthquake migration and coupled recurrence intervals, *Science*, *260*, 973–976.

Scholz, C. H. (2000), Evidence for a strong San Andreas Fault, *Geology*, *28*, 163–166.

Seeber, L., and J. G. Armbruster (1995), The San Andreas Fault system through the Transverse Ranges as illuminated by earthquakes, *J. Geophys. Res.*, *100*, 8285–8310.

Shaw, J. H., and P. M. Shearer (1999), An elusive blind-thrust fault beneath metropolitan Los Angeles, *Science*, *283*, 1516–1518.

Shaw, J. H., R. E. Bischke, and J. Suppe (1994), Relations between folding and faulting in the Loma Prieta epicentral zone: Strike-slip fault-bend folding, *U.S. Geol. Surv. Prof. Pap.*, *1550*, 3–21.

Shen, Z.-K., D. Dong, T. Herring, K. Hudnut, D. Jackson, R. King, S. McClusky, and L. Sung (1997), Geodetic measurements of southern California crustal deformation (abstract), *Eos Trans. AGU*, *78*(46), Fall Meet. Suppl., F477, F482.

Sieh, K. E. (1978), Prehistoric large earthquakes produced by slip on the San Andreas Fault at Pallett Creek, California, *J. Geophys. Res.*, *83*, 3907–3939.

Spotila, J. A., and K. Sieh (2000), Architecture of transpressional thrust faulting in the San Bernardino Mountains, southern California, from deformation on a deeply weathered surface, *Tectonics*, *19*(4), 589–615.

Stein, R. S., and T. C. Hanks (1998), M > 6 earthquakes in southern California during the 20th century: No evidence for a seismicity or moment deficit, *Bull. Seismol. Soc. Am.*, *88*, 635–652.

Suppe, J. (1983), Geometry and kinematic of fault-bend folding, *Am. J. Sci.*, *283*, 684–721.

Toda, S., and R. S. Stein (2002), Response of the San Andreas fault to the 1983 Coalinga-Nuñez earthquakes: An application of interaction-based probabilities for Parkfield, *J. Geophys. Res.*, *107*(B6), 2126, doi:10.1029/2001JB000172.

Toda, S., R. S. Stein, P. A. Reasenberg, J. H. Dieterich, and A. Yoshida (1998), Stress transferred by the 1995 M_w = 6.9 Kobe, Japan, shock: Effect on aftershocks and future earthquake probabilities, *J. Geophys. Res.*, *103*, 24,543–24,565.

Townend, J., and M. D. Zoback (2001), Implications of earthquake focal mechanisms for the frictional strength of the San Andreas fault system, *Geol. Soc. London Spec. Publ.*, *186*, 13–21.

Wald, D. J., T. S. Heaton, and K. W. Hudnut (1996), The slip history of the 1994 Northridge, California, earthquake determined from strong ground motion, teleseismic, GPS, and leveling data, *Bull. Seismol. Soc. Am.*, *86*, S49–S70.

Weldon, R. J., and K. E. Sieh (1985), Holocene rate of slip and tentative recurrence interval for large earthquakes on the San Andreas fault in Cajon Pass, southern California, *Geol. Soc. Am. Bull.*, *96*, 793–812.

Yule, D., and K. Sieh (2001), The paleoseismic record at Burro Flats: Evidence for a 300-year average recurrence for large earthquakes on the San Andreas fault in San Gorgonio Pass, southern California, paper presented at the 97th Annual Meeting, Geol. Soc. Am. Cordilleran Sect., Pac. Sect. Am. Assoc. Petrol. Geol., Universal City, Calif.

Yule, D., and K. Sieh (2003), Complexities of the San Andreas fault near San Gorgonio Pass: Implications for large earthquakes, *J. Geophys. Res.*, *108*(B11), 2548, doi:10.1029/2001JB000451.

S. Carena and J. Suppe, Department of Geosciences, Guyot Hall, Princeton University, Princeton, NJ 08544, USA. (scarena@princeton. edu; suppe@princeton.edu)

H. Kao, Pacific Geoscience Centre, Geological Survey of Canada, 9860 West Saanich Road, Sidney, B. C., Canada, V8L 4B2. (hkao@nrcan.gc.ca)

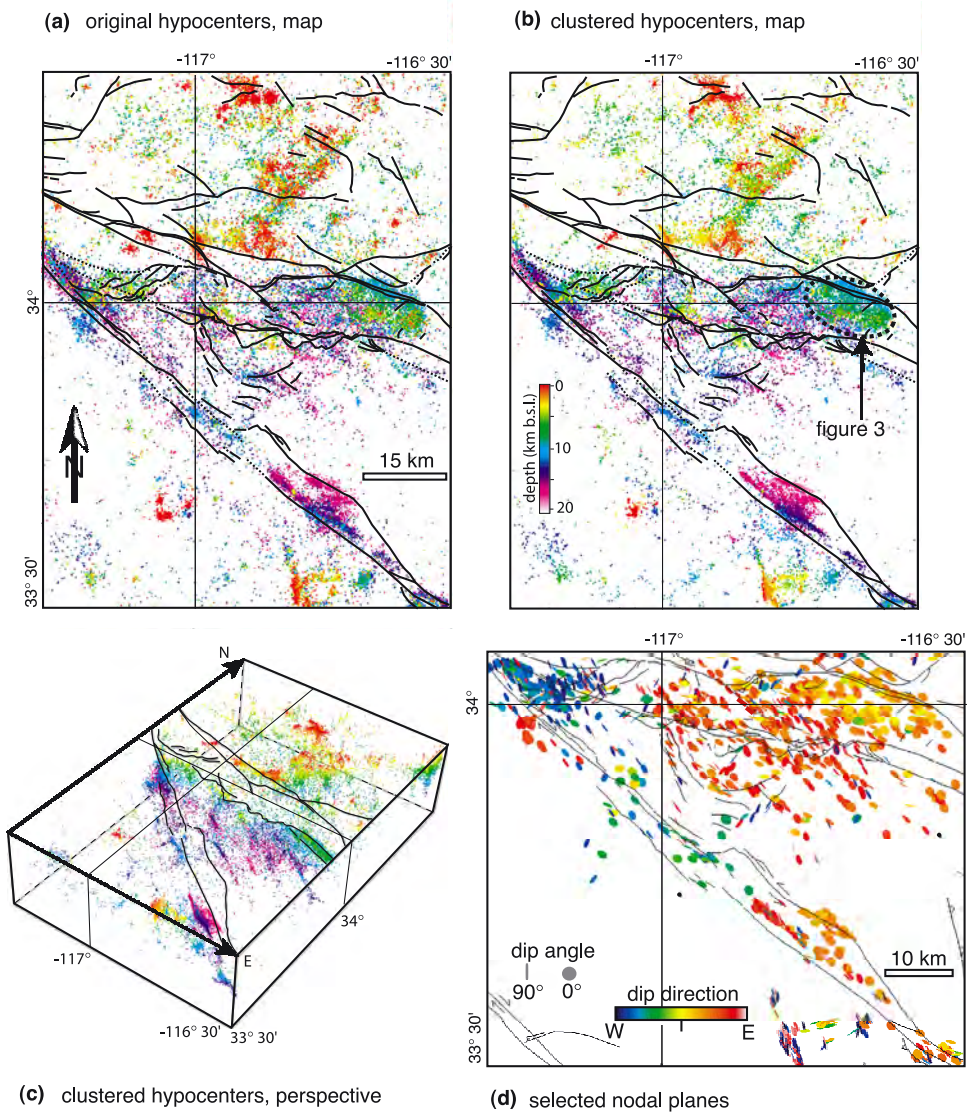

Figure 2. Data used in this paper. (a) Map of 43,000 events relocated by *Richards-Dinger and Shearer* [2000], before clustering. (b) Map of the same hypocenters after clustering. (c) The relocated hypocenters viewed in 3-D from the southeast. (d) Our selection of 1540 nodal planes from the focal mechanisms of *Hauksson* [2000]. This figure is supplemented by the "earthquake data" video.

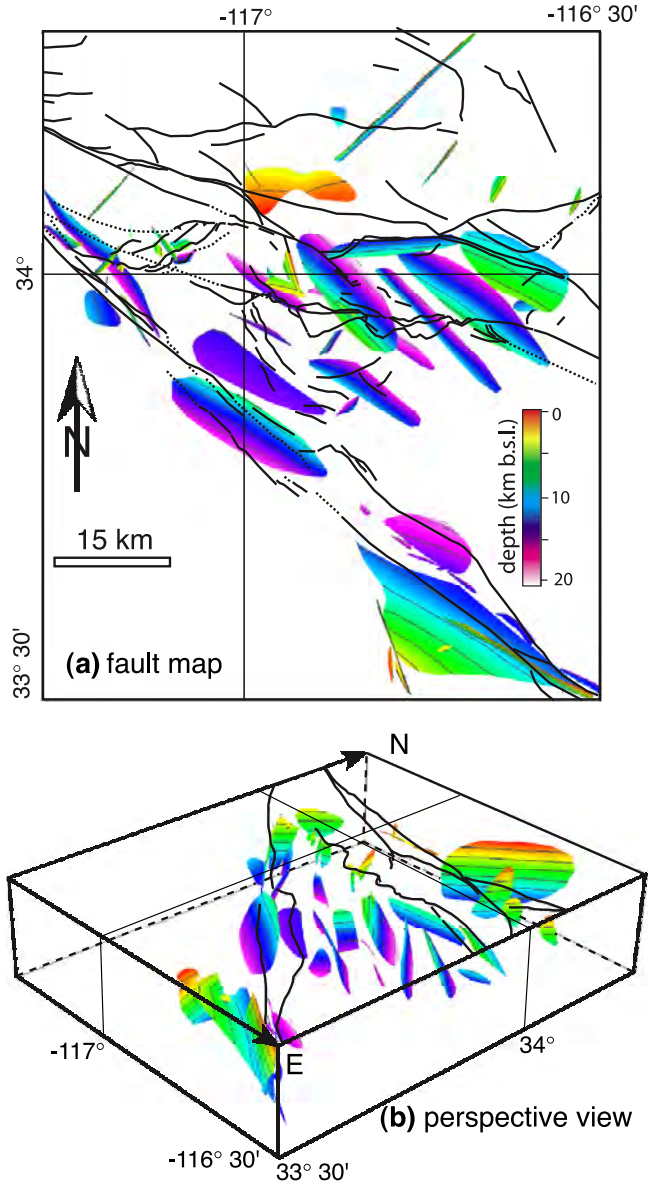

Figure 4. (a) Map and (b) view from the southeast of about 60 fault surfaces we modeled from the events shown in Figure 2. Color indicates depth, and contour spacing on faults is 3 km.

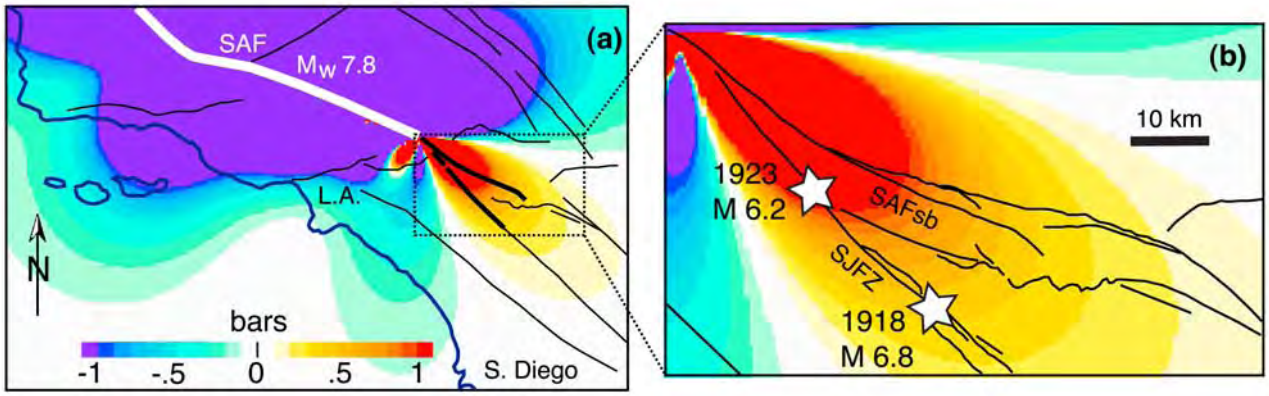

Figure 11. "Fort Tejon" earthquake scenario. (a) Coulomb stress changes caused by a hypothetical rupture of the San Andreas Fault north of Cajon Pass (SAF) in an event like the 1857 great Fort Tejon earthquake. (b) The effects are calculated on the San Jacinto fault zone (SJFZ) and the San Bernardino segment of the San Andreas Fault (SAFsb). This event would cause a stress increase >0.4 bars on the SAFsb and most of the SJFZ. Following the 1857 event, two earthquakes occurred on the SJFZ in 1918 and 1923. For this figure and all subsequent ones, calculation depth = 6 km, coefficient of friction = 0.4.

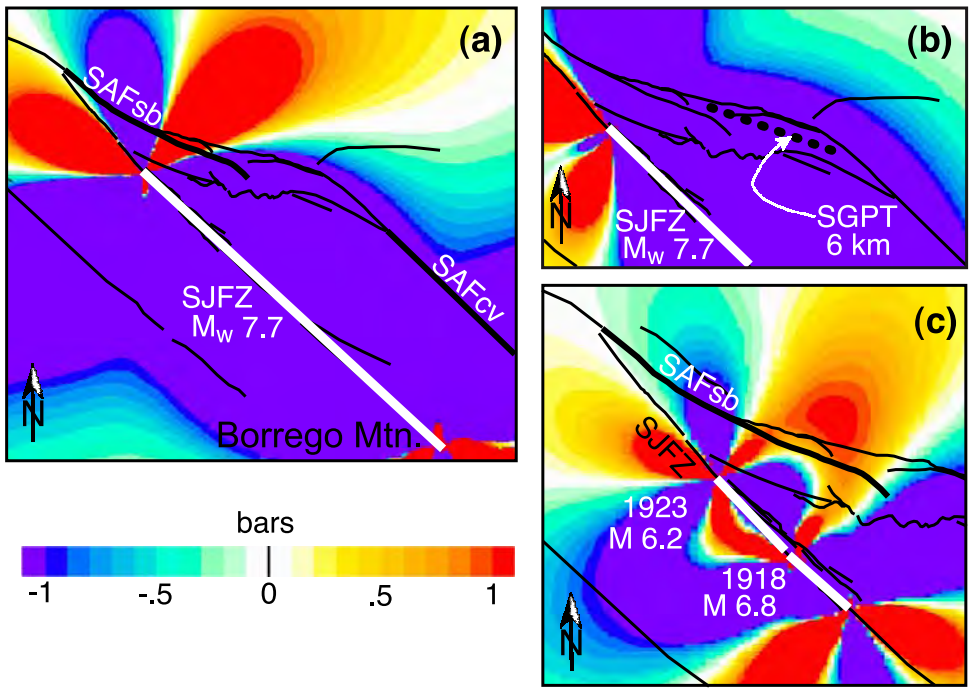

Figure 13. "San Jacinto" earthquake scenario. Coulomb stress changes caused by a hypothetical M_w 7.7 earthquake on the San Jacinto fault zone (SJFZ), calculated (a) on San Bernardino segment of the San Andreas Fault (SAFsb) and on the Coachella valley segment of the San Andreas Fault (SAFcv) and (b) on the San Gorgonio Pass thrust (SGPT). Stress is greatly decreased on the SAFcv and the SGPT, while both positive and negative changes affect the SAFsb. (c) Smaller earthquakes on the northern part of SJFZ have a similar effect on the SAFsb. Events on SJFZ thus tend to inhibit ruptures of the SAF system south of Cajon Pass.

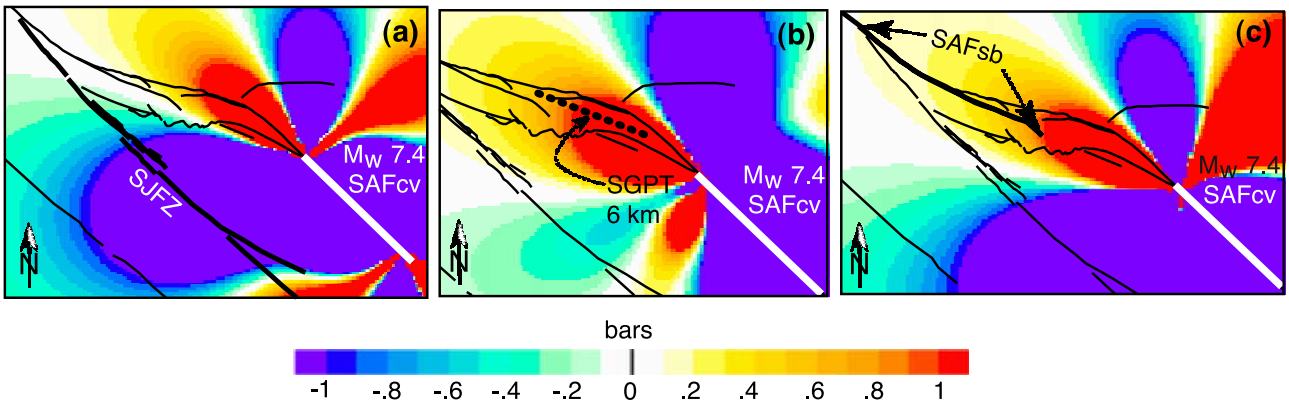

Figure 14. "Coachella" earthquake scenario. Coulomb stress changes caused by a hypothetical M_w 7.4 earthquake on the Coachella valley segment of the San Andreas Fault (SAFcv), calculated (a) on the San Jacinto fault zone (SJFZ), (b) on the San Gorgonio Pass thrust (SGPT), and (c) on the San Bernardino segment of the San Andreas Fault (SAFsb). While an event on the SAFcv would inhibit rupture on the SJFZ, it would at the same time bring the entire San Gorgonio Pass stepover (SAFbn + SGPT + SAFsb) closer to failure.

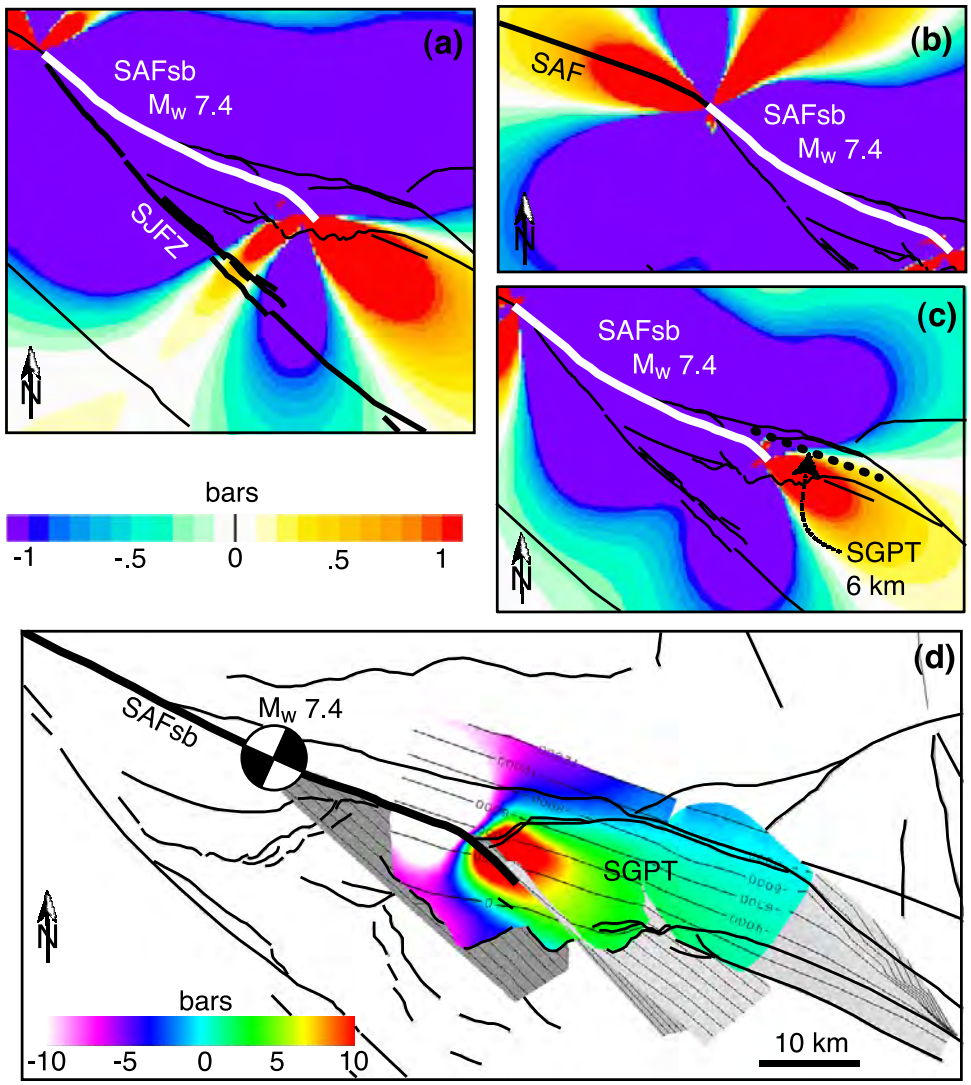

Figure 15. "San Bernardino-San Gorgonio" earthquake scenario. Coulomb stress changes caused by a hypothetical M_w 7.4 earthquake on the San Bernardino segment of the San Andreas Fault (SAFsb), calculated (a) on the San Jacinto fault zone (SJFZ), (b) on the Mojave segment of the San Andreas (SAF), and (c, d) on the San Gorgonio Pass thrust (SGPT). Figure 15d shows the coulomb stress change on the SGPT in 3-D, plotted on the fault surface itself. In this scenario the SAF northwest of Cajon Pass and the SGPT would be moved closer to failure, while ruptures on the SJFZ would be mostly inhibited.